Award Number: W81XWH-10-1-0115

TITLE: Photodynamic Molecular Beacons: An Image-Guided Therapeutic Approach to Breast Cancer Vertebral Metastases

PRINCIPAL INVESTIGATOR: Tracy WB Liu

CONTRACTING ORGANIZATION: University Health Network
Toronto, ON Canada M5G 2C4

REPORT DATE: March 2012

TYPE OF REPORT: Annual Summary

PREPARED FOR: U.S. Army Medical Research and Materiel Command
Fort Detrick, Maryland 21702-5012

REPORT DOCUMENTATION PAGE

Form Approved
OMB No. 0704-0188

1. REPORT DATE	2. REPORT TYPE	3. DATES COVERED
March 2012	Annual Summary	15 February 2011 – 14 February 2012

4. TITLE AND SUBTITLE

Photodynamic Molecular Beacons: An Image-Guided Therapeutic Approach to Breast Cancer Vertebral Metastases

5a. CONTRACT NUMBER

5b. GRANT NUMBER
W81XWH-10-1-0115

5c. PROGRAM ELEMENT NUMBER

6. AUTHOR(S)

Tracy WB Liu

E-Mail: tliu@uhnres.utoronto.ca

5d. PROJECT NUMBER

5e. TASK NUMBER

5f. WORK UNIT NUMBER

7. PERFORMING ORGANIZATION NAME(S) AND ADDRESS(ES)

University Health Network
Toronto, ON Canada M5G 2C4

8. PERFORMING ORGANIZATION REPORT NUMBER

9. SPONSORING / MONITORING AGENCY NAME(S) AND ADDRESS(ES)
U.S. Army Medical Research and Materiel Command
Fort Detrick, Maryland 21702-5012

10. SPONSOR/MONITOR'S ACRONYM(S)

11. SPONSOR/MONITOR'S REPORT NUMBER(S)

12. DISTRIBUTION / AVAILABILITY STATEMENT
Approved for Public Release; Distribution Unlimited

13. SUPPLEMENTARY NOTES

14. ABSTRACT

The vertebral column is the most common site of breast cancer metastases. Metastases disrupts the dynamic balance between bone resorption (by osteoclasts) and bone formation (by osteoblasts), inducing a vicious cycle whereby tumors reprogram osteoclasts causing osteolysis and promote tumor growth. The overexpression of MMPs in the vicious tumor-bone cycle not only aid tumors to spread to distant sites, but are also involved in the local dissolution of the vertebral body and tumor progression. Current therapies for managing vertebral metastases have significant limitations due to high associated risk of spinal cord damage. An attractive alternative is photodynamic therapy (PDT) for ablating breast cancer spinal metastases to relieve pain and prevent tumor progression and adjuvant to vertebroplasty, can stabilize weak and fractured vertebrae. However, current photosensitizers are limited by their non-specific accumulation. Photodynamic molecular beacons (PPMMPB), activated by MMPs, offer another level of PDT selectivity by preserving the spinal cord. Using a clinically-relevant metastatic model, PPMMPB-PDT results in the specific destruction of metastases while the spinal cord is left undamaged using a 150J light dose, a light dose 3 times greater than that achievable by the photosensitizer, Visudyne®. PPMMPB-PDT appears to not only destroy metastatic tumours but also osteoclasts thereby disrupting the viscious tumour-bone osteolytic cycle increasing the success of vertebroplasty.

15. SUBJECT TERMS
Breast Cancer, Vertebral Metastases, Photodynamic Therapy, Protease Activatable Beacons, Matrix Metalloproteinase, Optical Imaging

16. SECURITY CLASSIFICATION OF:			17. LIMITATION OF ABSTRACT	18. NUMBER OF PAGES	19a. NAME OF RESPONSIBLE PERSON
a. REPORT	b. ABSTRACT	c. THIS PAGE			USAMRMC
U	U	U	UU	33	19b. TELEPHONE NUMBER *(include area code)*

Table of Contents

Page

Introduction:

Breast cancer is a leading killer in North America. Approximately 85% of breast cancer patients with metastatic disease will develop bone metastases, in which the vertebral column is the most common site for metastatic formation.[1, 2] Breast cancer metastasis disrupts the dynamic balance between bone resorption by osteoclasts and bone formation by osteoblasts, inducing a vicious cycle whereby tumor cells reprogram osteoclasts, leading to osteolysis and promotion of tumor growth.[1, 3] Matrix metalloproteinases (MMPs) are a family of structurally-related, zinc-dependent endopeptidases implicated in the invasion and metastasis of cancer.[4-7] The upregulation of MMPs is critically involved in the destruction of the delicate balance between bone formation and degradation, reducing bone integrity (Fig. 1).[1, 3] Hence, MMPs not only aid the spread of tumor cells to distant sites, but are also involved in the local dissolution of the vertebral body and promote tumor progression within the vertebrae. Patients with spinal metastases have a high risk of spinal cord compression, resulting in motor dysfunction, neurological compromise and an overall poor prognosis.[1, 3] The associated 5-year survival rate in patients with spinal metastases is below 20% compared to a 5-year survival rate over 85% in patients with early stage breast cancer.[8] Regardless of the symptoms, all patients suffering from spinal metastases experience a substantial decrease in their quality of life.

Surgery and radiation therapy are the main treatment options for these patients. Surgical treatments, however, carry a high risk of morbidity due to the proximity of the spinal cord, while radiation therapy is limited to a level far below the optimal therapeutic dose because of the low tolerance of the spinal cord.[9] Clinical studies of radiotherapy have reported recurrence of symptoms, and pain relief is not experienced until at least 3 months after treatment.[10] Lastly, although pain relief and, in part, tumor regression are addressed by radiation treatment, spinal instability is not. Therein lies the need for improved therapies that specifically targets metastatic tumor cells while preserving the spinal cord to address pain relief, tumor regression and mechanical instability of the spine. PDT is an approved cancer treatment modality that destroys target cells when light activates a non-toxic photosensitizer (PS) to generate cytotoxic excited-state (singlet) oxygen.[11-13] It has several potential advantages over current cancer treatments due to its minimally-invasive nature, selectivity, ability to treat patients with repeated doses without initiating resistance or exceeding total-dose limitations, fast healing that results in little or no scarring, the ability to administer in an outpatient setting, minimal associated side effects and lack of contraindication with other modalities.[11-13] PDT has shown promising reports for destroying spinal metastases, particularly to debulk lesions as an adjuvant to vertebroplasty or kyphoplasty in order to mechanically stabilize weak or fractured vertebrae:[14-19] These surgical procedures involve injection of a plastic compound or placement of an inflatable balloon into the vertebral body, which is often limited by the space-occupying tumor mass. It was reported that not only can PDT (using the clinical photosensitizer Visudyne®) ablate spinal metastatic tumors,[14] but unexpectedly it also enhances vertebral mechanical stability.[18, 19] However, current photosensitizers are limited by their non-specific accumulation in normal tissues: e.g., Visudyne has non-specific uptake in the spinal cord limiting the therapeutic window which, in turn, reduces the aggressiveness of treatment in order to stay well within safe dose limits.[14, 15] Clearly, preservation of the spinal cord's structure and function is critical in the management of vertebral metastases.

Photodynamic molecular beacons (PMB) are a potential solution and provide an additional mechanism of selectivity in PDT over and above current photosensitizer and light targeting.[20] The beacons comprise a photosensitizer and a quencher moiety, linked, in the present case, by a MMP-cleavable peptide. They remain 'optically silent', i.e. photodynamically inactive, until

transformed into an activated state through cleavage of the linker, upon which both the PDT activity and PS fluorescence are restored, the latter providing the potential for real-time image guidance.[20] As beacons are only activated in the presence of these MMP metastases-specific proteases, normal tissues, including the spinal cord, should remain relatively protected (Figure 1).[20] Our vision is for PMB-PDT to result in complete destruction of intravertebral metastatic tumors without risk of spinal cord damage. This will have a potentially positive effect on bone integrity, increase the success and efficacy of vertebroplasty for spinal stabilization and eliminate local tumor recurrence. The intended impact of this novel intervention is the significant improvement in the quality of life for patients suffering from spinal metastases.

Body:

Preclinical studies evaluating PDT beacon' efficacy for treating spinal metastases: The therapeutic window of PMB-PDT was evaluated using a clinically relevant breast cancer metastases model (Fig. 2): $1x10^6$ luciferase and GFP transfected human breast cancer cells (MT-1) metastasize to the vertebral column 1-2 weeks following intracardiac injection into 4-5 week old female athymic rats (Hsd:RH-*Foxn1*^{rnu}) [14-19, 21]. Bioluminescence imaging using a Xenogen IVIS imaging system has been shown by us [14, 15, 17-19] and others [22, 23] as a powerful and quantitative tool to monitor bone metastases in small animals. Vertebral metastases were confirmed by bioluminescence imaging. A 2 hour drug-light interval was already established based upon our previous results [24]. Several parameters in the PMB-PDT treatment were evaluated including beacon concentration (1.5 mg/kg vs 3 mg/kg), light dose (150J vs 100J) and light fluence rate (80mW vs 100mW). Evaluated outcomes included 48 h post-treatment bioluminescence of remaining viable tumour, histomorphometric assessment of tumour burden, and neurologic evaluation. All animals using a 4 hr drug-light interval with a 3 mg/kg concentration of PMB, 100mW and 150J light dose demonstrated hindlimb paralysis and thus, a 2 hour drug-light interval was used further. Within 24 hours after PDT, at least 25% of rats demonstrated different degrees of paresis (i.e. hindleg lameness) and decreased sensitivity in all groups using fluence rates of 100mW regardless of the overall light dose or PMB concentration (fig. 3). These animals were immediately euthanized. The bioluminescent signals decreased in the treated area over 48 h, with both increasing photosensitizer dose at fixed light energy and vice versa. There was considerable variability in the initial signal intensity of vertebrae targeted for treatment. However, statistically significant differences were observed in the tumour growth when the control groups were compared to the treatment groups ($p < 0.05$); tumour growth was calculated by taking the ratio of the bioluminescent signal 48 hours post treatment versus the bioluminescent signal pre-treatment (Fig. 4). The routine pathologic examination of the H&E-stained slides included the appearance of the tumour cells and the presence of polymorphonuclear cells, apoptotic and necrotic tumour cells, as well as hemorrhage and signs of vascular changes in the vertebra. Surprisingly, TRAP (titrate-resistant acid phosphatase) staining of osteoclasts demonstrated that in areas of PDT induced tumour cell destruction also resulted in the destruction of osteoclasts demonstrating that PMB-PDT not only destroys spinal metastases but also disrupts the viscious tumour-bone osteolytic cycle (Fig.5). The doses required for tumour ablation whilst avoiding collateral neurologic damage in this model appears to be a 3 mg/kg concentration of PMB using a 2 hour drug-light interval and applied light energy of 150J using a fluence rate of 80mW to treat the spine. This treatment light dose is 2 times the light energy used when compared to previous PDT treatments using Visudyne®[14]. Thus, we have demonstrated PMB's ability to specifically destroy spinal metastases in our animal model while better preserving neurological damage.

Beacon Development: A current limitation of evaluating PMBs *in vivo* is the inability to evaluate their pharmacokinetics and pharmacodynamics due to the inherently silent nature of beacons. A potential solution is the use of radiolabeling as radioactivity cannot be silenced nor limited by tissue thickness as fluorescence imaging is. For proof of concept, the ability and ease of incorporating copper-64 (^{64}Cu) into a targeted porphyrin probe transforming a theranostic agent into a PET imaging radiotracer was demonstrated. Using a previously developed folate receptor (FR)-targeted optical imaging and PDT agent, porphyrin-GDEVDGSGK-folate (PPF, Figure 6), [25] the ease and stability of ^{64}Cu chelation into pyropheophorbide- α was evaluated. Porphyrins have several ideal characteristics as ^{64}Cu chelators: their aforementioned stable ^{64}Cu-chelating ability [26] the clinically-validated minimal toxicity of ^{64}Cu-prophyrin [27], the compatible half-lives of ^{64}Cu and the pharmacokinetics of porphyrin [28, 29], and the fact that ^{64}Cu-chelation does not alter the biodistribution of the host porphyrin [29, 30]. The half-life of ^{64}Cu ($t_{1/2}$ = 12.7 h) provides adequate time for radiolabeling chemistry and imaging over 24-48 h to accommodate PPF accumulation at targeted sites [25]. PPF was easily dissolved in an aqueous solution with a small amount of DMSO (≤ 1%) and was radiolabeled efficiently in 0.1M ammonium acetate buffer at 60°C for 10-20 min (Figure 7a) [30]. The success of the ^{64}Cu labeling was determined by radio-UPLC (Ultra Performance Liquid Chromatography) using a C18 column. Using simultaneous multichannel monitoring of the Pyro-specific UV absorbance at 410 nm and a radioactive signal, the incorporation of ^{64}Cu into PPF was observed. As expected, no free ^{64}Cu was detected during the radiolabeling procedure, based on the radio-UPLC radioactive channel chromatography (Figure 7b) [30]. The radiolabeling yield was > 99.9% and the radiochemical purity of ^{64}Cu-PPF was > 98% and the specific activity was 2.66×10^6 GBq/mol. MicroPET imaging and MicroCT scans were performed accordingly at 4 and 24 h post-injection. The favorable tumor-to-background ratio of ^{64}Cu-PPF is evident in Figure 8A [30]. ^{64}Cu-PPF easily delineates the tumor from all other tissues by PET. Inhibition imaging studies were conducted by co-injection of the radiotracer with 500-fold excess folic acid. Figure 8B demonstrates that the uptake of ^{64}Cu-PPF at the tumor site was significantly blocked by excess folic acid, indicating that ^{64}Cu-PPF targeting is FR-mediated [30]. Biodistribution studies of ^{64}Cu-PPF in the KB xenograft models at 4 and 24 h post-injection were also performed (Fig.8C) [30]. All vital organs (including heart, liver, spleen, kidney, lung, stomach, large-intestine, small intestine, adrenal, brain, muscle and bone) and tumors were removed, washed with normal saline and weighed for radioassay. The highest uptake was in the kidneys, corresponding to the PET imaging results. Tumor uptake was 3.02 ± 0.55 % injected dose (ID)/g at 4 h and 1.64 ± 0.33 %ID/g at 24 h post injection (Figure 8C) [30]. However, the tumor-to-muscle ratio of ^{64}Cu-PPF was 3.47 ± 0.47 at 4 h and 8.88 ± 3.60 at 24 h post injection (Figure 8D), demonstrating the fast clearance of ^{64}Cu-PPF in non-target tissues while ^{64}Cu-PPF is retained within the tumor [30]. Through the present study, we hope to revitalize this field of radio-metalloporphyrin, based on the demonstration of transforming PPF into ^{64}Cu-PPF, a targeted PET imaging probe for FR-positive tumors. We have shown the ease and efficient radiolabeling of Pyro with ^{64}Cu, while retaining its favorable biodistribution, pharmacokinetics and selective tumor uptake, characteristics that were first demonstrated optically. Clearly, the 12.7 h half-life of ^{64}Cu is compatible with the pharmacokinetics of Pyro, providing adequate time for both the radiolabeling chemistry and accumulation of the photosensitizer at tumor sites. Lastly, we report the first stable chelation of ^{64}Cu with a chlorophyll moiety, Pyro. The use of ^{64}Cu chelation of Pyro may be employed for prediction and quantitative measurements of photosensitizer accumulation in tumors to aid in

treatment planning and monitoring of PDT treatments. Radiolabeling of Pyro also provides a more accurate and quantitative measurement of the probe's in vivo biodistribution, due to the difficulty of absolute quantification of fluorescence in vivo. This is especially promising as a solution to overcoming the current limitation of PMBs. The radiolabeling procedure and stability of ^{64}Cu chelation into Pyro will be easily incorporated into PMBs as it is very similar to PPF (peptide-folate versus peptide-quencher).

Key Research Accomplishments:

- Determined the therapeutic window of PMB-PDT achieving appreciable tumour ablation while avoiding collateral neurologic damage (3mg/kg PMB, 2 hr drug-light interval, <80mW and 150J)
- Demonstrated that PMB-PDT not only destroy spinal metastases but also destroy involved osteoclasts further disrupting the viscious osteolytic tumour-bone cycle
- Determined and demonstrated the ease and stability of chelating 64Cu to Pyro in a folate-targeted Pyro probe while retaining its favorable biodistribution, pharmacokinetics and selective tumor uptake, characteristics that were first demonstrated optically which can be easily translatable to PMBs due to the similarity of the probes.

Reportable Outcomes:

- Manuscript: Liu, T.W., Akens, M.K., Chen, J, Wise-Milestone, L., Wilson, B.C., Zheng, G. *Photodynamic Molecular Beacons in Breast Cancer Vertebral Metastases: Imaging Validation of Beacon Specificity*. Bioconjug Chem. (2011), 22(6):1021-30.
- Manuscript: Liu, T.W., Shi, J., Chen, J., Green, D., Jaffray, D., Wilson, B.C., Wang, F., Zheng, G. *Transforming a Targeted Porphyrin Theranostic Agent into a PET Imaging Probe for Cancer.* Theranostics. (2011), 1:363-70.
- Abstract: Liu, T.W.., Stewart, J.M., Chen, J., Shi, J., MacDonald T.D., Neel, B.G., Wilson, B.C. and Zheng G. "Evaluating Primary Human Ovarian Cancer using a targeted multi-modal theranostic agent." Poster presentation, Photonics West, Jan 2012, San Francisco, USA.
- Abstract: Liu, T.W., Akens, M.K., Chen, J, Wise-Milestone, L., Wilson, B.C., Zheng, G, "Photodynamic Molecular Beacons: Image-Guided Therapeutic Approach for Vertebral Metastases. " Oral Presenation, European Society of Photobiology, Sept. 2011, Geneva Switzerland.
- Abstract: Liu, T.W.., Stewart, J.M., Chen, J., Shi, J., MacDonald T.D., Neel, B.G., Wilson, B.C. and Zheng G. "Evaluating Primary Human Ovarian Cancer using a targeted multi-modal theranostic agent." Poster presentation, European Society of Photobiology, Sept. 2011, Geneva Switzerland.
- Abstract: Liu, T.W., Akens, M.K., Chen, J, Wise-Milestone, L., Wilson, B.C., Zheng, G, "Photodynamic Molecular Beacons: Image-Guided Therapeutic Approach for Vertebral Metastases. " Oral and poster presentation, DOD Era of Hope, Aug 2011, Florida, USA.
- Abstract: Liu, T.W., Akens, M.K., Chen, J, Wise-Milestone, L., Wilson, B.C., Zheng, G, "Specific activation of photodynamic molecular beacons: an image-guided therapeutic approach for vertebral metastases." Oral presentation, European Conferences on Biomedical Optics, May 2011, Munich, Germany.
- Abstract: Liu, T.W., Akens, M.K., Chen, J, Wise-Milestone, L., Wilson, B.C., Zheng, G, "Specific Activation of Photodynamic Molecular Beacons: An Image -Guided

Therapeutic Approach for Vertebral Metastases." Awarded Top Poster Presentation, 5th International Graduate Summer School Biophotonics '11, May 2011,Backafallsbyn, Ven in Sweden.

Conclusion:

Photodynamic molecular beacons may be a key component in the use of PDT as a new, minimally-invasive, safe and effective therapy for the management of patients with spinal metastases when used, for example, as an adjuvant to minimally-invasive surgical techniques such as vertebroplasty or kyphoplasty for mechanical stabilization.(*14, 16, 17*) We have recently started a Phase I clinical trial with the clinically-approved photosensitzer Visudyne (QLT Inc, 8Vancouver, BC, Canada), in which the objective is to debulk the intravertebral space-occupying tumor mass that often impedes these surgical approaches. However, based on preclinical studies(*14, 15*), the therapeutic window is likely to be limited by the non-specific uptake of the photosensitizer by healthy tissues, including the spinal cord, which will restrict the drug and light doses that can be used safely. PMBs potentially address this limitation. We have demonstrated the specific activation of PMBs by MMP-expressing vertebral metastases in a relevant preclinical model illustrating defined kinetics and the ability to target intravertebral metastatic tumors with minimal uptake or activation in the spinal cord. This is a first step in the further development of such beacons and their potential translation into useful clinical tools for a range of applications. To this end, as mentioned above, we have demonstrated a therapeutic window for PMB-PDT which achieves appreciable tumour ablation while avoiding collateral neurologic damage. Currently, we are evaluating the potential of delivering PMBs locally to avoid further off-target activation and provide a more clinically feasible means of deliverying PMBs. In parallel, with the continual development of PMBs (^{64}Cu chelation, incorporation of zippers), our vision is for PMBs to result in complete destruction of intravertebral metastatic tumors without risk of spinal cord damage. This will have a potentially positive effect on bone integrity, increase the success and efficacy of vertebroplasty for spinal stabilization and eliminate local tumor recurrence. The intended impact of this novel intervention is the significant improvement in the quality of life for patients suffering from spinal metastases.

References:

1. Siclari, V.A., T.A. Guise, and J.M. Chirgwin, *Molecular interactions between breast cancer cells and the bone microenvironment drive skeletal metastases.* Cancer Metastasis Rev, 2006. **25**(4): p. 621-33.
2. Kingsley, L.A., et al., *Molecular biology of bone metastasis.* Mol Cancer Ther, 2007. **6**(10): p. 2609-17.
3. Mundy, G.R., *Metastasis to bone: causes, consequences and therapeutic opportunities.* Nat Rev Cancer, 2002. **2**(8): p. 584-93.
4. Brinckerhoff, C.E. and L.M. Matrisian, *Matrix metalloproteinases: a tail of a frog that became a prince.* Nat Rev Mol Cell Biol, 2002. **3**(3): p. 207-14.
5. Kessenbrock, K., V. Plaks, and Z. Werb, *Matrix metalloproteinases: regulators of the tumor microenvironment.* Cell. **141**(1): p. 52-67.
6. Woodward, J.K., et al., *The roles of proteolytic enzymes in the development of tumour-induced bone disease in breast and prostate cancer.* Bone, 2007. **41**(6): p. 912-27.
7. Guise, T.A., *Breaking down bone: new insight into site-specific mechanisms of breast cancer osteolysis mediated by metalloproteinases.* Genes Dev, 2009. **23**(18): p. 2117-23.
8. American Cancer Society. Breast Cancer Facts & Figures 2009-2010. Atlanta: American Cancer Society, I.
9. Finn, M.A., F.D. Vrionis, and M.H. Schmidt, *Spinal radiosurgery for metastatic disease of the spine.* Cancer Control, 2007. **14**(4): p. 405-11.
10. Bartels, R.H., Y.M. van der Linden, and W.T. van der Graaf, *Spinal extradural metastasis: review of current treatment options.* CA Cancer J Clin, 2008. **58**(4): p. 245-59.
11. Wilson, B.C. and M.S. Patterson, *The physics, biophysics and technology of photodynamic therapy.* Phys Med Biol, 2008. **53**(9): p. R61-109.
12. Celli, J.P., et al., *Imaging and photodynamic therapy: mechanisms, monitoring, and optimization.* Chem Rev, 2010. **110**(5): p. 2795-838.
13. Pervaiz, S. and M. Olivo, *Art and science of photodynamic therapy.* Clin Exp Pharmacol Physiol, 2006. **33**(5-6): p. 551-6.
14. Akens, M.K., et al., *Defining the therapeutic window of vertebral photodynamic therapy in a murine pre-clinical model of breast cancer metastasis using the photosensitizer BPD-MA (Verteporfin).* Breast Cancer Res Treat, 2010. **119**(2): p. 325-33.
15. Akens, M.K., et al., *Photodynamic therapy of vertebral metastases: evaluating tumor-to-neural tissue uptake of BPD-MA and ALA-PpIX in a murine model of metastatic human breast carcinoma.* Photochem Photobiol, 2007. **83**(5): p. 1034-9.
16. Burch, S., et al., *Photodynamic therapy for the treatment of vertebral metastases in a rat model of human breast carcinoma.* J Orthop Res, 2005. **23**(5): p. 995-1003.
17. Burch, S., et al., *Photodynamic therapy for the treatment of metastatic lesions in bone: studies in rat and porcine models.* J Biomed Opt, 2005. **10**(3): p. 034011.
18. Won, E., et al., *Effects of photodynamic therapy on the structural integrity of vertebral bone.* Spine (Phila Pa 1976), 2010. **35**(3): p. 272-7.
19. Won, E., et al., *Beyond bisphosphonates: photodynamic therapy structurally augments metastatically involved vertebrae and destroys tumor tissue.* Breast Cancer Res Treat, 2010.
20. Zheng, G., et al., *Photodynamic molecular beacon as an activatable photosensitizer based on protease-controlled singlet oxygen quenching and activation.* Proc Natl Acad Sci U S A, 2007. **104**(21): p. 8989-94.
21. Burch, S., et al., *Multimodality imaging for vertebral metastases in a rat osteolytic model.* Clin Orthop Relat Res, 2007. **454**: p. 230-6.
22. Klerk, C.P., et al., *Validity of bioluminescence measurements for noninvasive in vivo imaging of tumor load in small animals.* Biotechniques, 2007. **43**(1 Suppl): p. 7-13, 30.
23. Sato, A., B. Klaunberg, and R. Tolwani, *In vivo bioluminescence imaging.* Comp Med, 2004. **54**(6): p. 631-4.
24. Liu, T.W., et al., *Imaging of specific activation of photodynamic molecular beacons in breast cancer vertebral metastases.* Bioconjug Chem, 2011. **22**(6): p. 1021-30.
25. Stefflova, K., et al., *Peptide-based pharmacomodulation of a cancer-targeted optical imaging and photodynamic therapy agent.* Bioconjug Chem, 2007. **18**(2): p. 379-88.
26. Wrenn, F.R., Jr., M.L. Good, and P. Handler, *The use of positron-emitting radioisotopes for the localization of brain tumors.* Science, 1951. **113**(2940): p. 525-7.

27. Bases, R., S.S. Brodie, and S. Rubenfeld, *Attempts at tumor localization using Cu 64-labeled copper porphyrins*. Cancer, 1958. **11**(2): p. 259-63.
28. Wilson, B.C., et al., *Chromatographic analysis and tissue distribution of radiocopper-labelled haematoporphyrin derivatives* Laser Med Sci, 1988. **3**(1-4): p. 71-80.
29. Firnau, G., et al., *64Cu labelling of hematoporphyrin derivative for non-invasive in-vivo measurements of tumour uptake.* Prog Clin Biol Res, 1984. **170**: p. 629-36.
30. Hambright, P., et al., *The distribution of various water soluble radioactive metalloporphyrins in tumor bearing mice.* Bioinorg Chem, 1975. **5**(1): p. 87-92.
31. Liu, T.W., Shi, J., Chen, J., Green, D., Jaffray, D., Wilson, B.C., Wang, F., Zheng, G. *Transforming a Targeted Porphyrin Theranostic Agent into a PET Imaging Probe for Cancer.* Theranostics, 2011. **1**: p. 363-70.

Appendices:

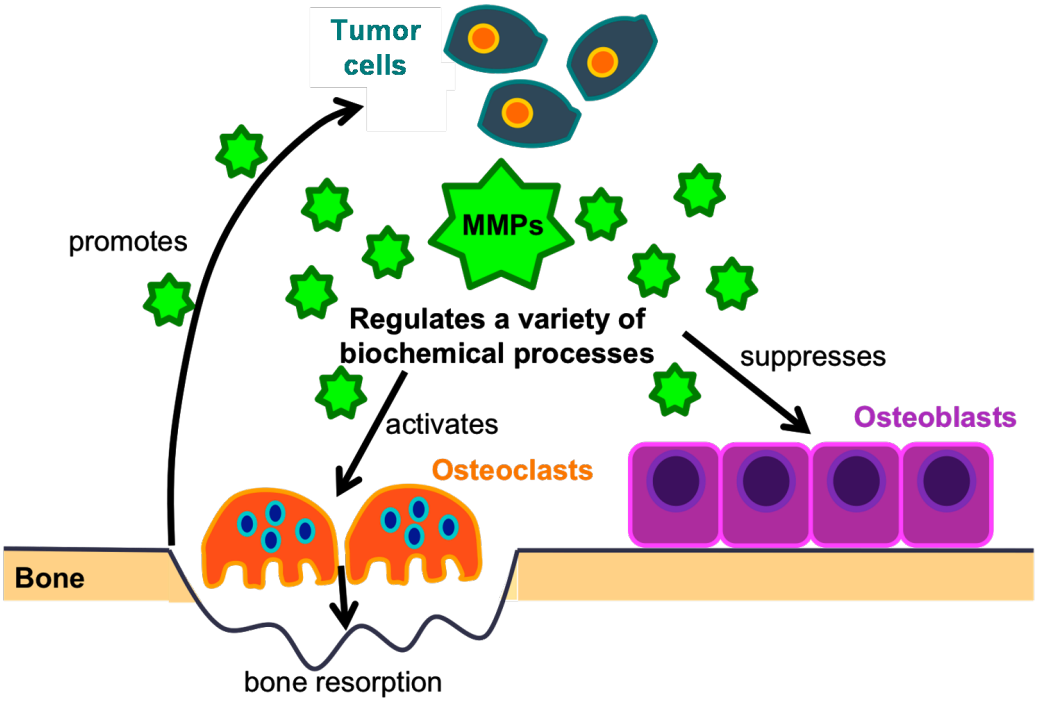

Figure 1A. MMP involvement in the tumor-bone vicious cycle. MMPs directly promote tumor progression but also indirectly promote tumor progression by activation of osteoclasts and suppressing osteoblasts.

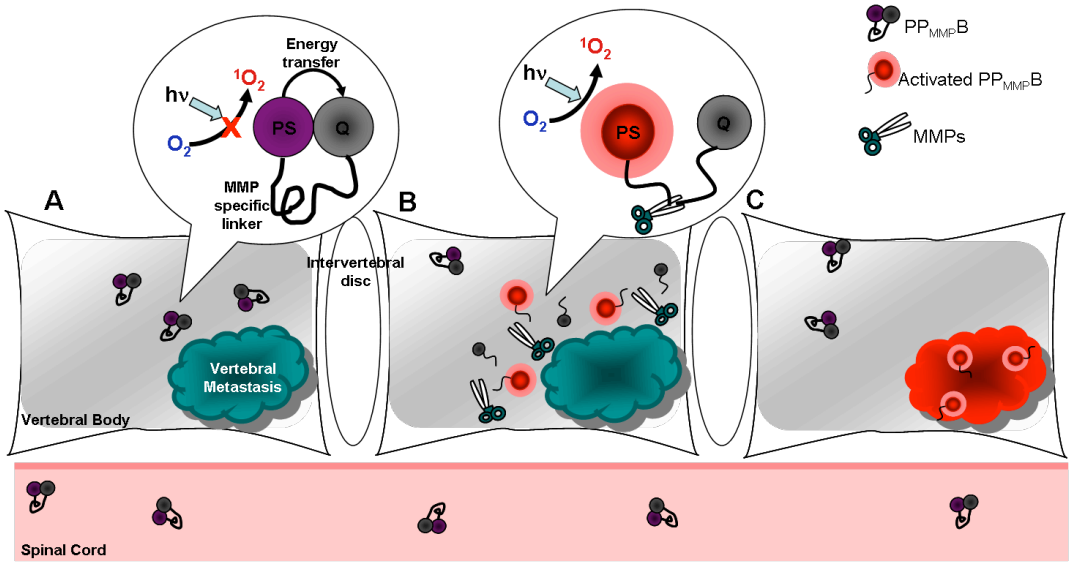

Figure 1B. Schematic of photodynamic molecular beacon (PP$_{MMP}$B) activation by vertebral metastases. The beacon accumulates in tissue but remains photodynamically and optically silent (A) until cleaved by MMPs at sites of vertebral metastases (B), which restores both its fluorescence for imaging and generation of singlet oxygen for treatment (C).

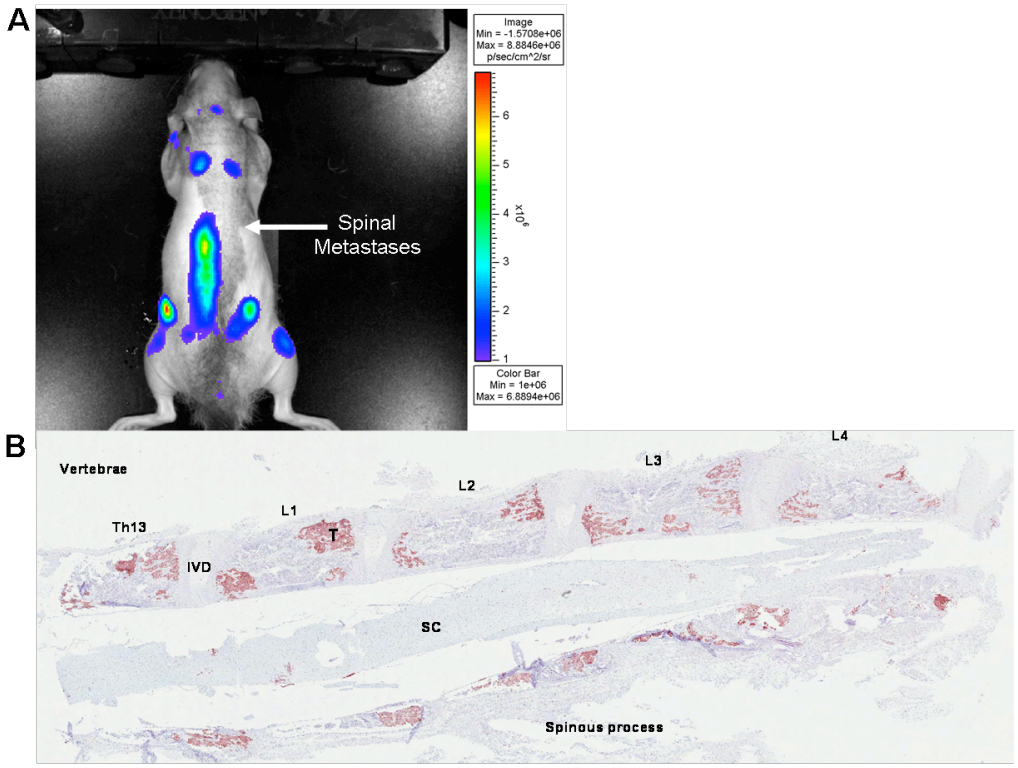

Figure 2. *In vivo* breast cancer vertebral metastases model. A) Example of bioluminescent imaging of MT-1 vertebral metastases development at 14 days after intracardiac injection of 1x10^{6}cells, showing multiple sites of metastitic growth, including in the spine.. B) Example of immunohistology section of vertebral column where hEGFr immunhisto stains for viable tumor (red sections) (T- tumor, SC - spinal cord, IVD - intervertebral disc, L - lumbar, Th - thoracic)

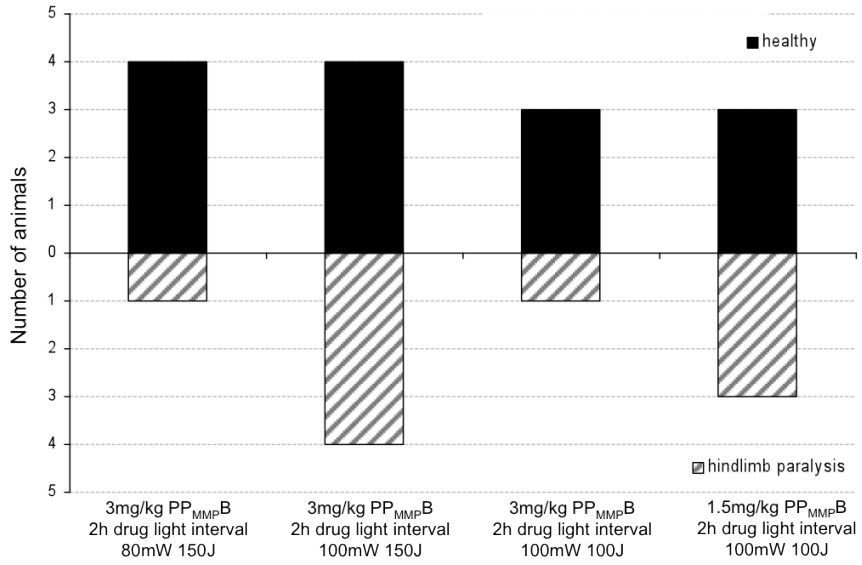

Figure 3. Number of animals that were healthy versus affected by hindlimb paralysis after the different treatment groups. When 100mW fluence rate was used regardless of the light dose and PP$_{MMP}$B concentration, hindlimb paralysis was seen in at least 25% of animals treated.

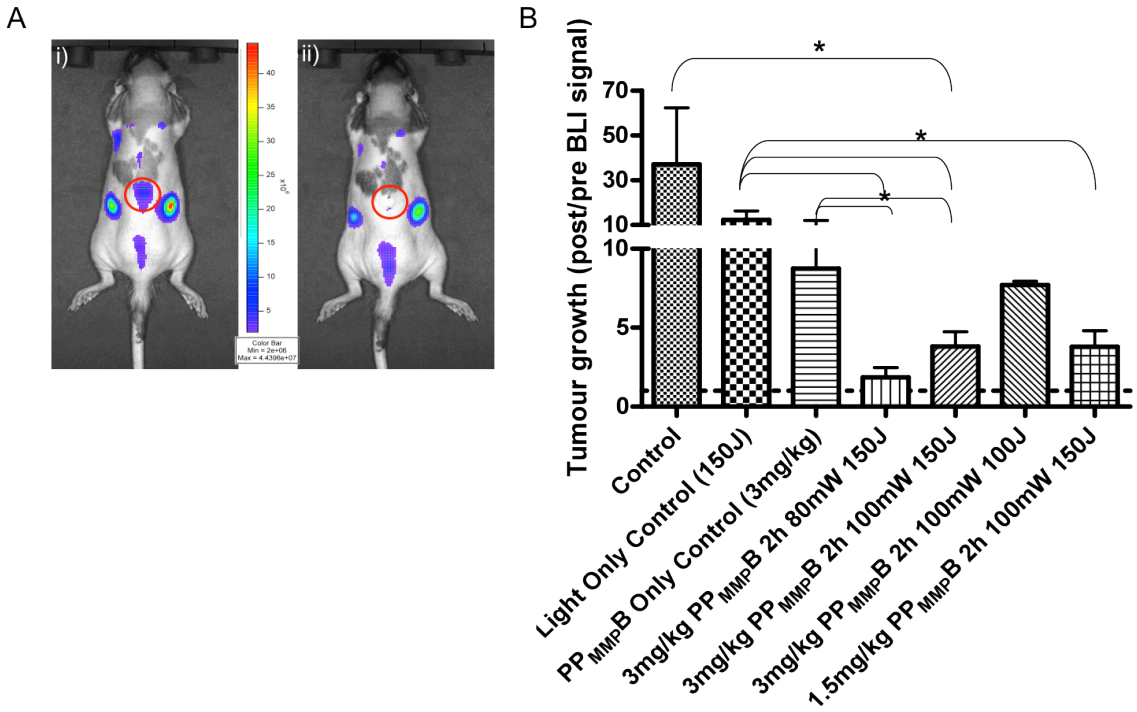

Figure 4. Spinal metastases growth. A) Representative BLI imaging of MT-1 vertebral metastases i) pre PDT versus ii) 48h post PDT where red circle indicates treated area. B) Summary of average tumour growth based upon change in bioluminescent signal in different treatment groups where 48h post PDT treatment signals are normalized to BLI signals before treatment Note: * indicates statistically significant difference ($p < 0.05$). BLI - bioluminescent

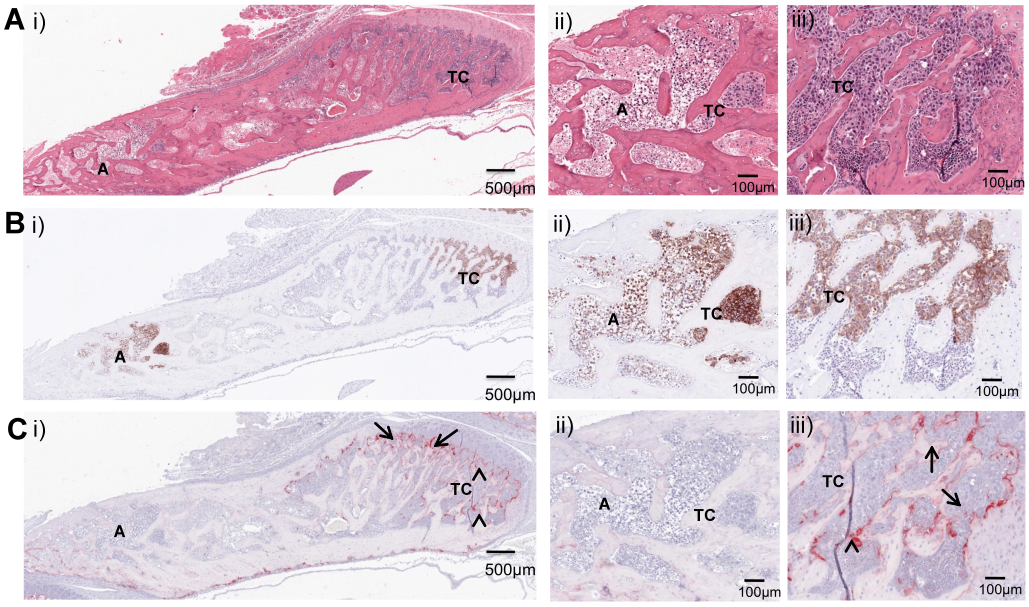

Figure 5. Histology of spines after PDT treatment confirm PDT induced therapeutic effect where A represents H&E staining of a treated vertebrae, B represents EGFR immunohistological staining and C represents TRAP (titrate-resistant Acid Phosphatase) staining of the corresponding area. An entire vertebrae is shown in i) where as ii) represents a magnified area of PDT induced damage and iii) represents a magnified area of tumour growth without PDT induced damage.

Note: A - Apoptotic and necrotic tumour cells, TC - Intact tumor cells and →osteoclasts

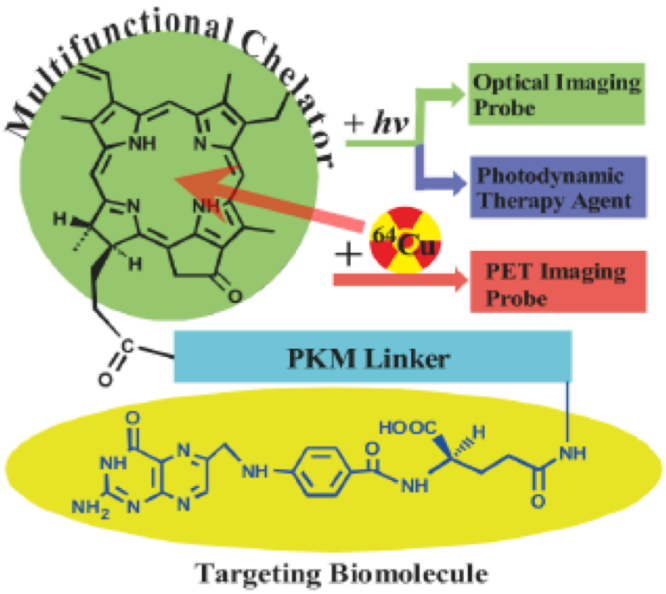

Figure 6. The structure design of the PPF (Pyro-PKM Linker-Folate, molecular weight of 1800 g/mol). Here the PKM linker (pharmacokinetics modifying linker) is the peptide sequence, GDEVDGSGK.

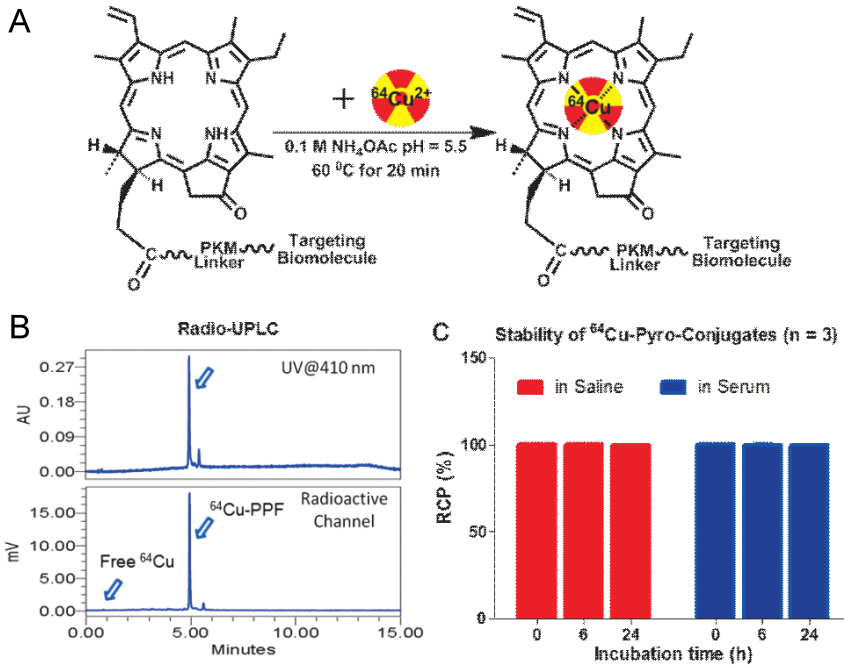

Figure 7. The radiolabeling procedure, quality control and stability of ^{64}Cu-PPF. A) The scheme of the ^{64}Cu-radiolabeling of Pyro-Conjugates, B) quality control of ^{64}Cu-labeled PPF by radio-UPLC, C) *in vitro* stability of ^{64}Cu-Pyro-Conjugates in saline or serum (10% FBS) solution (RCP = The radiochemical purity of ^{64}Cu-Pyro-Conjugates) (n = 3).

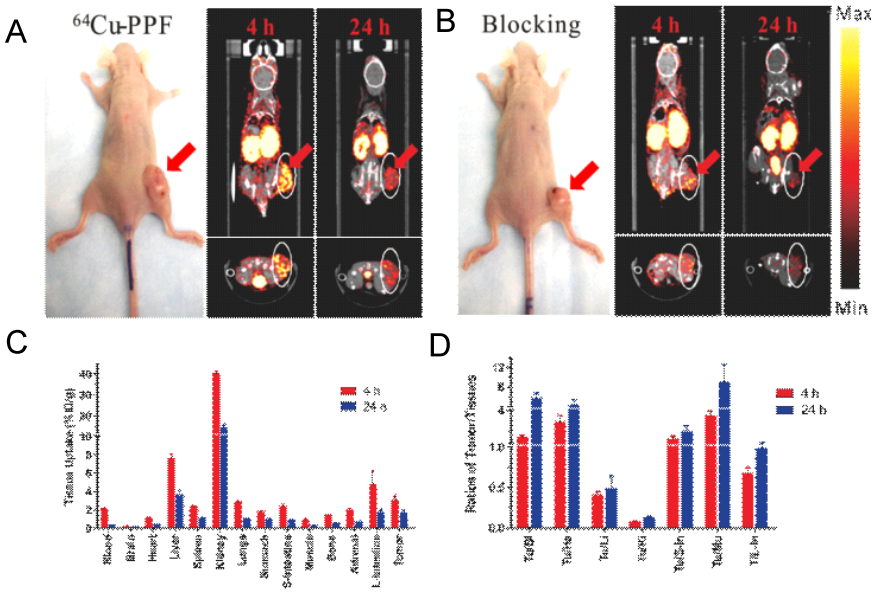

Figure 8. MicroPET/CT imaging and biodistribution. a) Representative MicroPET/CT images (coronal images (top) and single transverse slices passing through the tumors (bottom)) of KB tumor-bearing mice (n = 3) at 4, 24 h after intravenous injection of ^{64}Cu-PPF. b) Images, including coronal images (top) and single transverse slices passing through the tumors (bottom), obtained with pre-injection (0.5 h earlier) of 500-fold excess folic acid for blockade (n = 1). c) Tissue uptake of ^{64}Cu-PPF in selected organs at 4 h (red bars) and 24 h (blue bars) after intravenous injection. d) Ratios of tumor-to-selected organs in mice administered with ^{64}Cu-PPF at 4 h (red bars) and 24 h (blue bars) post injection. Data are presented as means ± 1 SD (n = 3).

Bioconjugate Chemistry

COMMUNICATION

pubs.acs.org/bc

Imaging of Specific Activation of Photodynamic Molecular Beacons in Breast Cancer Vertebral Metastases

Tracy W. Liu,[†,‡] Margarete K. Akens,[§] Juan Chen,[‡] Lisa Wise-Milestone,[§] Brian C. Wilson,[†,‡] and Gang Zheng*[,†,‡]

[†]Department of Medical Biophysics, University of Toronto, Canada

[‡]Ontario Cancer Institute, University Health Network, Canada

[§]Sunnybrook Health Science Centre, Canada

Supporting Information

ABSTRACT:

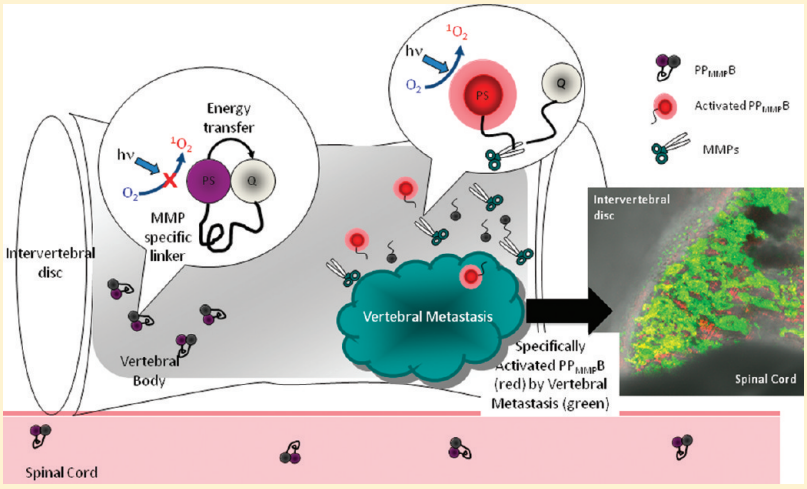

Breast cancer is the second leading cause of cancer-related death in women. Approximately 85% of patients with advanced cases will develop spinal metastases. The vertebral column is the most common site of breast cancer metastases, where overexpression of matrix metalloproteinases (MMPs) promotes the spread of cancer. Current therapies have significant limitations due to the high associated risk of damaging the spinal cord. An attractive alternative is photodynamic therapy providing noninvasive and site-selective treatment. However, current photosensitizers are limited by their nonspecific accumulation. Photodynamic molecular beacons ($PP_{MMP}B$), activated by MMPs, offer another level of PDT selectivity and image-guidance preserving criticial tissues, specifically the spinal cord. Metastatic human breast carcinoma cells, MT-1, were used to model the metastatic behavior of spinal lesions. *In vitro* and *in vivo* evidence demonstrates MMP specific activation of $PP_{MMP}B$ in MT-1 cells. Using a clinically relevant metastatic model, fluorescent imaging establishes the specific activation of $PP_{MMP}B$ by vertebral metastases versus normal tissue (i.e., spinal cord) demonstrating the specificity of these beacons. Here, we validate that the metastasis-selective mechanism of $PP_{MMP}Bs$ can specifically image breast cancer vertebral metastases, thereby differentiating tumor and healthy tissue.

INTRODUCTION

Metastatic spread of tumor cells is the most devastating attribute of cancer and is often the cause of mortality. Due to the unique microenvironment of the bone, it is the most common site of distant metastases from cancers of the breast, lung, kidney, thyroid, and prostate.[1] The bone provides a fertile environment for the growth of cancer and promotes the aggressive behavior of tumor cells, since the mineralized bone matrix houses many growth factors, bone-destroying osteoclasts and bone-forming osteoblasts.[1] Approximately 85% of breast cancer patients with metastatic disease will develop bone metastases, in which the vertebral column is the most common site for metastatic formation.[2,3] Matrix metalloproteinases (MMPs) are a family of structurally related, zinc-dependent endopeptidases implicated in the invasion and metastasis of cancer through the degradation of the basement membrane and collagen-rich extracellular matrix.[4−7] Furthermore, MMPs are exquisite regulators of the tumor microenvironment by

Received: April 1, 2011
Revised: May 16, 2011
Published: May 18, 2011

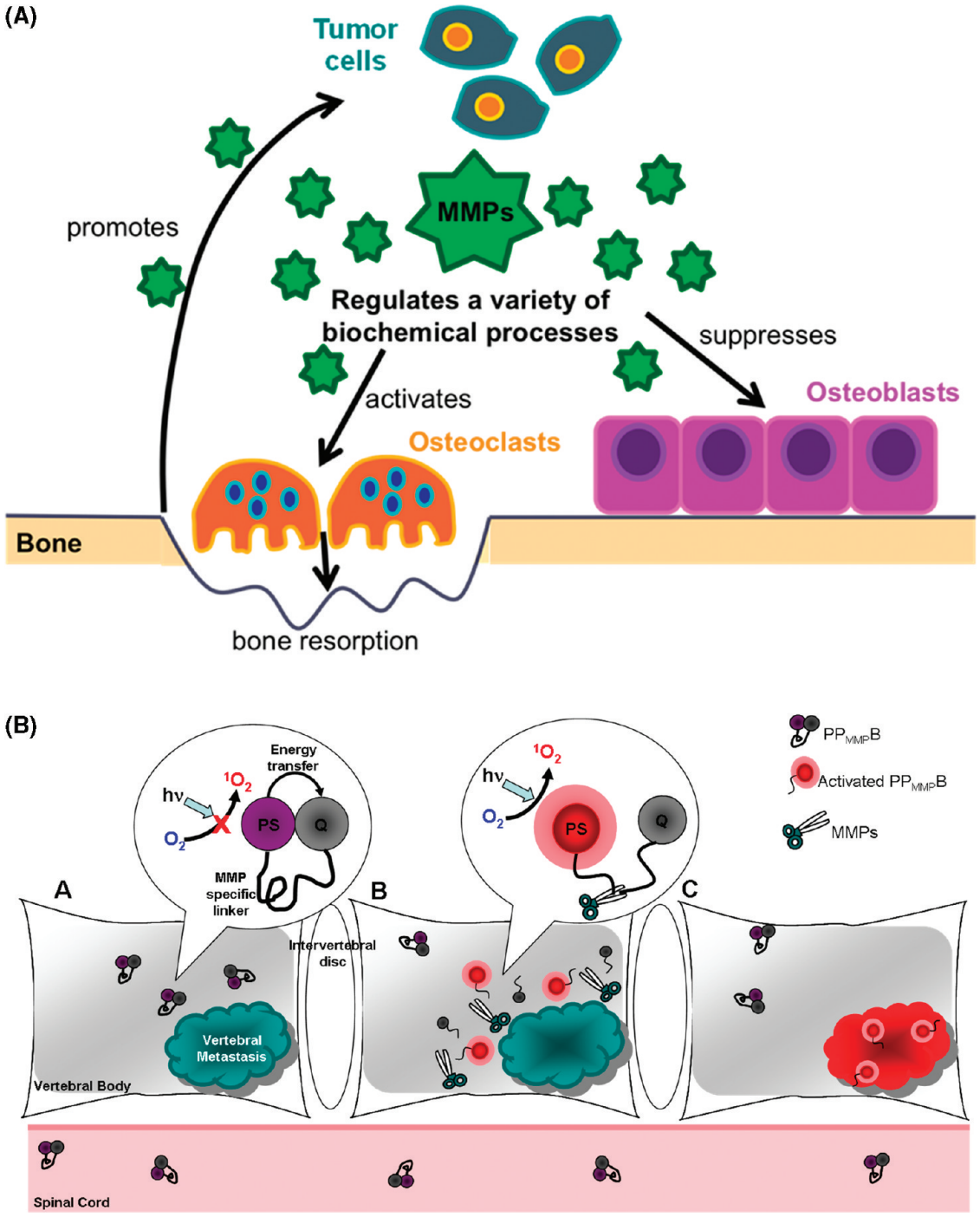

Figure 1. (A) MMP involvement in the tumor-bone vicious cycle. MMPs directly promote tumor progression but also indirectly promote tumor progression by activation of osteoclasts and suppressing osteoblasts. (B) Schematic of photodynamic molecular beacon ($PP_{MMP}B$) activation by vertebral metastases. The beacon accumulates in tissue but remains photodynamically and optically silent (A) until cleaved by MMPs at sites of vertebral metastases (B), which restores both its fluorescence for imaging and generation of singlet oxygen for treatment (C).

virtue of their ability to process many biological modulators, such as cytokines and growth factors within the bone matrix.[4−6]

Breast cancer spinal metastases are predominantly osteolytic (bone destructive), which is associated with an increase in osteoclast activity.[1] Metastasis disrupts the dynamic balance between bone resorption by osteoclasts and bone formation by osteoblasts, inducing a vicious cycle whereby tumor cells reprogram osteoclasts, leading to osteolysis and promotion of tumor growth.[1,2] MMPs play a vital role in signaling cascades involved in metastatic growth, and their upregulation leads to the processing of many growth factors, including TGF-β,[8] IGFs,[9] E-caderin,[10] and RANKL,[11] that are all essential for metastatic tumor progression within the vertebral body.[7,12,13] MMPs themselves also destroy healthy tissue, particularly in the bone, since the matrix is composed primarily of mineralized fibrillar type I collagen,[7] a main substrate of many MMPs. The upregulation of MMPs is thus critically involved in the

destruction of the delicate balance between bone formation and degradation, reducing bone integrity (Figure 1A).[1,2] Hence, MMPs not only aid the spread of tumor cells to distant sites, but are also involved in the local dissolution of the vertebral body and promote tumor progression within the vertebrae.

The resulting osteolysis causes bone pain, vertebral pathological fractures, progressive deformity, hypercalcemia, and spinal instability.[1,2] Patients with spinal metastases have a high risk of spinal cord compression, resulting in motor dysfunction, neurological compromise, and an overall poor prognosis.[1,2] The associated 5-year survival rate in patients with spinal metastases is below 20% compared to a 5-year survival rate over 85% in patients with early stage breast cancer.[14] Regardless of the symptoms, all patients suffering from spinal metastases experience a substantial decrease in their quality of life. Surgery and radiation therapy are the main treatment options for these patients. Surgical treatments, however, carry a high risk of morbidity due to the proximity of the spinal cord, while radiation therapy is limited to a level far below the optimal therapeutic dose because of the low tolerance of the spinal cord.[15] Clinical studies of radiotherapy have reported recurrence of symptoms, and pain relief is not experienced until at least 3 months after treatment.[16] Lastly, although pain relief and, in part, tumor regression are addressed by radiation treatment, spinal instability is not. Therein lies the need for improved therapies that specifically target metastatic tumor cells while preserving the spinal cord to address pain relief, tumor regression, and mechanical instability of the spine.

Protease activatable probes have been generating a great amount of promise for cancer imaging. They offer control of fluorescence emission in response to specific cancer targets and, thus, are useful tools for *in vivo* imaging. With our increasing knowledge about the human genome in health and disease, peptide-based "smart" probes are continually developed for *in vivo* optical imaging of specific molecular targets, biological pathways, and cancer progression. We introduced photodynamic molecular beacons which provide an additional therapeutic mechanism by exploiting the intrinsic fluorescence capabilities of photosensitizers.[17] Photosensitizers are light activated drugs used in photodynamic therapy (PDT). PDT is an approved cancer treatment modality that destroys target cells when light activates a nontoxic photosensitizer (PS) to generate cytotoxic excited-state (singlet) oxygen.[18−20] Photodynamic molecular beacons provide an additional mechanism of selectivity in PDT over and above the targeting afforded by current photosensitizers and specific light delivery.[17] This is illustrated in Figure 1B. The beacons comprise a photosensitizer and a quencher moiety, linked, in the present case, by a MMP-cleavable peptide ($PP_{MMP}B$). They remain "optically silent", i.e., photodynamically inactive, until transformed into an activated state through cleavage of the linker, upon which both the PDT activity and PS fluorescence are restored, the latter providing the potential for real-time image guidance.[17] Furthermore, as $PP_{MMP}Bs$ are only activated in the presence of these secreted tumor-specific proteases, normal tissues, including the spinal cord, should remain relatively protected.[17] One concern is that uptake of activated $PP_{MMP}Bs$ by the spinal cord may occur if activated beacons are allowed sufficient time to diffuse from the tumor to normal tissues. Here, as a first step in implementing $PP_{MMP}Bs$ as a therapeutic strategy for the management of vertebral metastases, we validate that the metastasis-selective mechanism of $PP_{MMP}Bs$ can specifically target breast cancer vertebral metastases, thereby differentiating tumor and healthy tissue.

MATERIALS AND METHODS

Study Design. $PP_{MMP}B$ activation was validated *in vitro* using the human MT-1 metastatic breast cancer cell line. Breast cancer tissue and cell lines have been shown to overexpress MMPs (Supporting Information Figure S1).[21,22] Preliminary *in vivo* activation was demonstrated in MT-1 xenografts grown subcutaneously on the flank of athymic mice. A scrambled beacon, $PP_{scrambled}B$, in which the peptide linker sequence is not cleavable by MMPs,[20] was used to validate the specific activation of $PP_{MMP}B$ by the MT-1 cells. As a relevant preclinical model of vertebral metastases, MT-1 cells were injected intracardially to establish metastases in athymic rats. The activation of $PP_{MMP}B$ within the spinal column was assessed at each of 2, 4, 12, and 24 h after intravenous injection of $PP_{MMP}B$. $PP_{MMP}B$ activation was further compared in tumor-bearing versus healthy animals, at 2 and 4 h post injection. The fixed dose of $PP_{MMP}B$ was 3 mg per kg bodyweight, equivalent to that using Visudyne in previous studies with this model.[23]

$PP_{MMP}B$ Synthesis. The $PP_{MMP}B$ consists of the photosensitizer Pyropheophorbide-α (PS) and black hole quencher 3 (Q), linked by the amino acid sequence GPL*G*LARK, which is an MMP-cleavable peptide: italics indicate the cleavage site. It was synthesized as described previously.[17] $PP_{scrambled}B$ comprises the same PS and Q but with a linker sequence, tsgpnqeqk, composed of D-amino acids that has been shown not to be cleaved by MMPs.[24]

Cells. MT-1 cells, a human metastatic breast cancer cell line, were kindly provided by Dr. O. Engebraaten, Norwegian Radium Hospital, Norway.[25,26] Cells were grown and maintained in Roswell Park Memorial Institute (RPMI) 1640 media supplemented with 10% fetal bovine serum at 37 °C in an atmosphere of 5% CO_2 in a humidified incubator. The MT-1 cells were stably transfected with a double-fusion plasmid (luciferase and green flurescent protein, GFP) kindly provided by Dr. Joseph Wu (Stanford University) and a lentivirus kindly provided by Dr Ren-Ke Li, (University of Toronto). The expression of GFP and luciferase provides a means to identify the cells and assess their viability.[23,27−31]

***In Vitro* Model.** *In vitro* activation of $PP_{MMP}B$ was evaluated by both confocal microscopy and flow cytometry. $PP_{MMP}B$ (2 nmol) or $PP_{scrambled}B$ (2 nmol) were first dissolved in 2% dimethyl sulfoxide, DMSO (Sigma Aldrich), and 0.025% Cremophore.[17] The solutions were then diluted with the culture medium to a final concentration of 10 μM (molecular weight of the $PP_{MMP}B$ is 1856 g/mol). 2×10^4 cells in 0.4 mL of culture medium per well were seeded in Nunc Laboratory-TekII-CC2 8-well chamber slides and incubated for 2 days at 37 °C under 5% CO_2 in a humidified incubator to grow to 80% confluency. $PP_{MMP}B$ activation after 6 h incubation of MT-1 cells was assessed using a laser scanning confocal microscope (Olympus FluoView 1000: 633 nm excitation, >650 nm detection). To quantify $PP_{MMP}B$ fluorescence activation and uptake in MT-1 cells, 2×10^5 cells in 2 mL of medium per well were inoculated in 6-well plates and incubated for 2 days at 37 °C under 5% CO_2 in a humidified incubator. The cells were then incubated with 1 mL of $PP_{MMP}B$ or $PP_{scrambled}B$ solution (10 μM) for 1 and 6 h, respectively (similar to previous studies[17]), at 37 °C under 5% CO_2. The beacon solution was then removed after the above incubation times and assessed by HPLC-MS to confirm the beacon cleavage. The cells were trypsinized from the well plates and transferred to a 15 mL centrifuging tube containing 2 mL PBS. The cells were centrifuged at 1000 rpm for 6 min and the

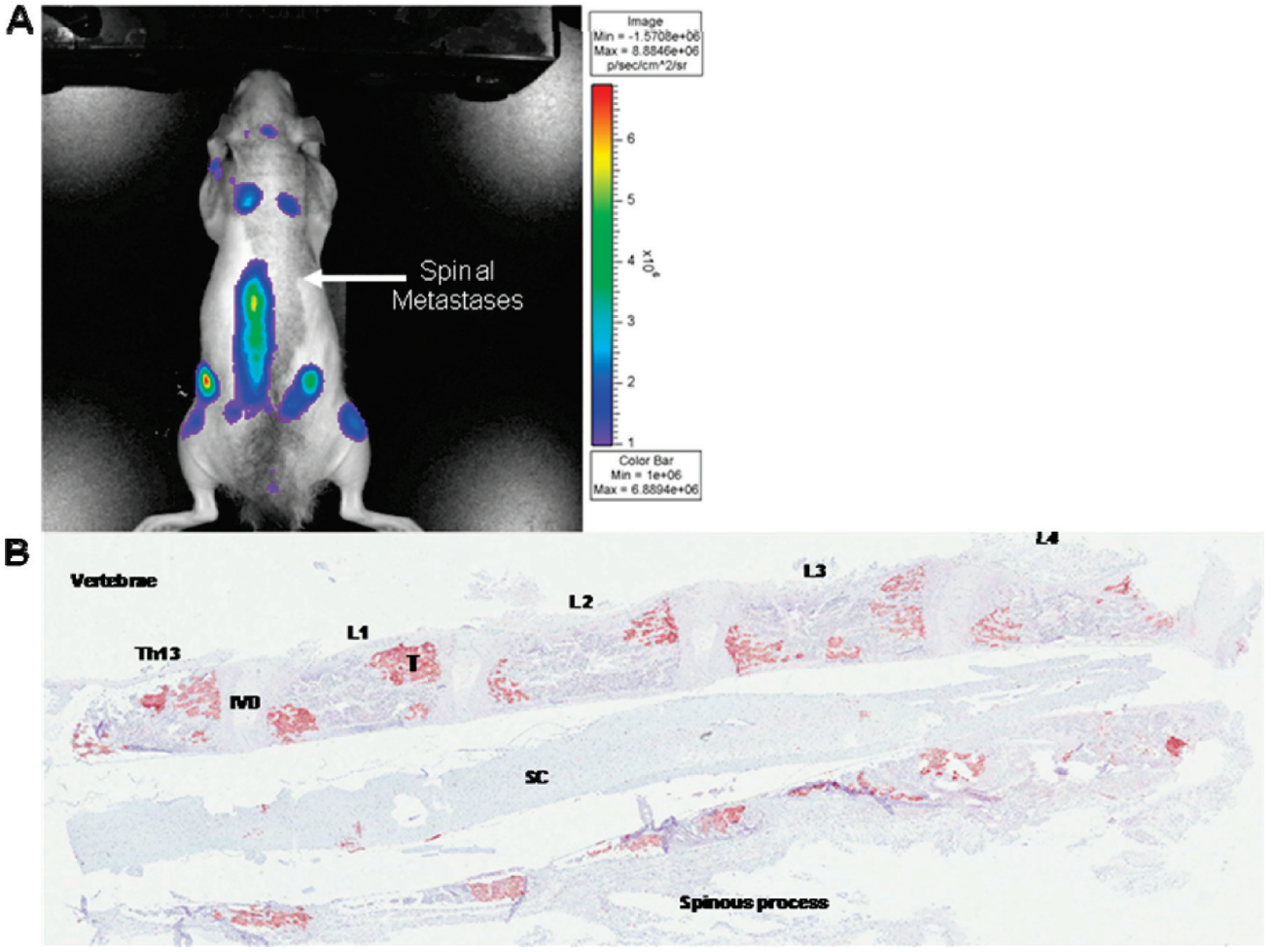

Figure 2. *In vivo* breast cancer vertebral metastases model. (A) Example of bioluminescent imaging of MT-1 vertebral metastases development at 14 days after intracardiac injection of 1×10^6cells, showing multiple sites of metastitic growth, including in the spine. (B) Example of immunohistology section of vertebral column where hEGFr immunhisto stains for viable tumor (red sections) (T - tumor, SC - spinal cord, IVD - intervertebral disk, L - lumbar, Th - thoracic).

PBS was removed. This rinsing procedure was repeated 3 times. The cells were fixed by a 2% paraformaldehyde solution for 10 min, after which they were centrifuged and rinsed twice with PBS. The fluorescence intensities of the cells were measured by flow cytometry (CytomicsFC 500, Beckman Coulter, CA, USA: 633 nm excitation, 660−690 nm detection). The maximum cell count was approximately 10 000 in each sample.

***In Vivo* Xenograft Model.** All animal studies were carried out under institutional approval (University Health Network, Toronto, Canada). Adult athymic female nude mice (Hsd:Athymic Nude-Foxn1^{nu}; Harlan, Indianapolis, IN, USA) were inoculated subcutaneously with 1×10^6 MT-1 cells in 200 μL of media in both the left and right flanks for intratumoral injection studies of $PP_{MMP}B$. To evaluate the activation of $PP_{MMP}B$ by a systemic injection, mice were inoculated similarly only on the right flank. Animals were maintained in pathogen-free conditions in autoclaved microisolator cages. After 2 weeks, by which time the tumors were 5−10 mm in diameter, the mice were fed a low-fluorescence diet (Harlan Tekland) for 4 days to reduce the autofluoresence background. A 2 mg/kg dose of $PP_{MMP}B$ or $PP_{scrambled}B$ (corresponding to the dose used in previous studies[17]) was formulated in 30 μL of aqueous solution with 2% DMSO and 0.5% Tween-80.[17] Under general anesthesia (isofluorane in oxygen), a 27G needle was used to inject this in multiple locations in the tumor to improve the distribution. A 2 mg/kg intravenous injection (tail vein) of $PP_{MMP}B$ was formulated in 150uL of aqueous solution with 2% DMSO and 0.5% Tween-80. Whole-body *in vivo* fluorescence imaging was performed before and at multiple time points after injection (Maestro, CRi: 650 nm excitation, ≥700 nm detection, auto-exposure integration time).

***Ex Vivo* Xenograft Studies.** MT-1 tumors harvested from mice 24 h following intratumor injections of beacon and were snap-frozen in liquid nitrogen and stored at −70 °C. Frozen sections (10 μm) were cut on a cryostat. After 5 min at room temperature, the slides were immersed in PBS for another 5 min, then dried, and 4 μL of mounting solution with DAPI, 4′,6-diamidino-2-phenylindole (Vector laboratories. Inc.), was added as a nuclear stain. The sections were covered by a coverslip and imaged by confocal microscopy similar to the *in vitro* studies above.

***In Vivo* Vertebral Metastases Model.** Female 5−6-week-old athymic rats (rnu/rnu; Harlan Sprague−Dawley, Indianapolis, IN, USA) were used as a model to mimick vertebral metastatic spread. The activation of $PP_{MMP}B$ was compared in the spinal column in tumor-bearing and healthy animals. Under general

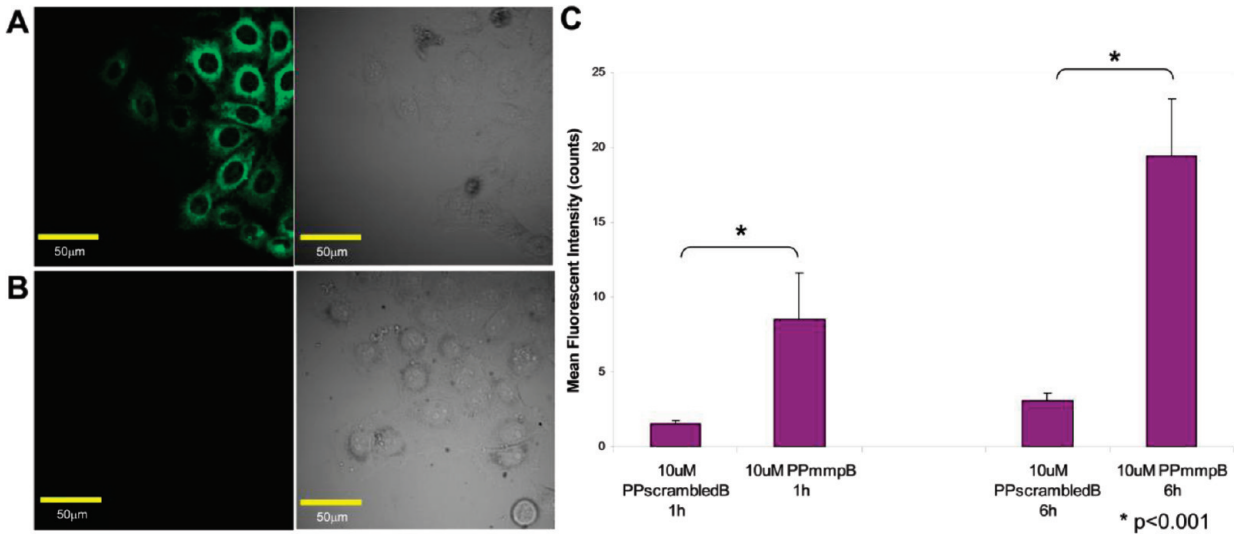

Figure 3. *In vitro* fluorescence and corresponding brightfield images of MT-1 cells after 6 h incubation in (A) 10 μM $PP_{MMP}B$, (B) 10 μM $PP_{scrambled}B$. (C) Comparison of the fluorescence intensity of MT-1 cells incubation with $PP_{MMP}B$ and $PP_{scrambled}B$ for 1 or 6 h monitored by flow cytometry ($n = 3$ samples, $p < 0.001$).

inhalation anesthesia (isofluorane in oxygen), MT-1 cells were injected intracardially at a concentration of 2×10^6 in 0.2 mL of RPMI 1640 media. Fourteen days later, *in vivo* bioluminescence imaging was performed as follows to confirm the establishment of metastases. Luciferin (Xenogen Corp., MA, USA) was dissolved in 0.9% NaCl at a concentration of 30 mg/mL and a single dose of 60 mg/kg was injected intraperitoneally into anaesthetized animals. Bioluminescent images were taken 15 min post luciferin injection where animals were placed ventrally in a whole-body bioluminescence imager (IVIS Spectrum: Caliper Life Sciences, CA, USA), integrating the counts over 30 s (Figure 2A). Following this, 3 mg/kg of $PP_{MMP}B$ (corresponding to equivalent Visudyne dose used in previous PDT studies[23,30,31]) in 2.5% DMSO, 0.5% Tween80 was injected through the tail vein and, at each time point above, cohorts were euthanized by pentobarbital overdose.

***Ex Vivo* Vertebral Metastases Studies.** At the time of necroscopy in these animals, the T13−L4 vertebrae were harvested intact, transferred to PBS, and immediately cut in the sagittal plane using a low-speed precision saw (IsoMet, Buehler, Illinois). $PP_{MMP}B$ activation by MT-1 vertebral tumors was assessed by confocal microscopy of the cut surface (633 nm excitation, >650 nm detection) at 10× magnification. These images were overlaid by corresponding GFP images from the MT-$1^{luc/GFP}$ cells (488 nm excitation, >520 nm detection), in order to evaluate the specific activation of $PP_{MMP}B$ *in vivo* by MT-1 metastases. Using commercial software (*Olympus Fluoview FV 1000*), the degree of colocalization of $PP_{MMP}B$ and MT-1 metastatic cells within the vertebral column was assessed by calculating the Pearson coefficient between the two fluorophores (activated $PP_{MMP}B$ and GFP), with −1 representing no overlap and +1 representing 100% concordance of localization. $PP_{MMP}B$ activation was quantified in these samples using the Maestro imaging system (650 nm excitation, ≥700 nm detection, autoexposure integration time), normalizing the total fluorescence signal within a defined region of interest (ROI) by the exposure time and the ROI area. The values used were based on the midsagittal images of the fluorescence within the vertebral body and the spinal cord, and the difference between these was compared using a Student *t* test. To confirm metastatic formation within the vertebral column, the spines were then fixed in 10% buffered formalin, decalcified, sectioned (10 μm), and stained either with H&E or immunhistochemically using a mouse-antihuman epidermal growth factor receptor (hEGFr) antibody (Zymed, Laboratories Inc., San Francisco, CA, USA). This antibody does not cross react with rat tissues, enabling specific visualization of the metastatic human breast cancer cells withzin the rat vertebral bone and bone marrow compartments (Figure 2B).

RESULTS

The *in vitro* specific activation of $PP_{MMP}B$ by MT-1 cells was compared with that of the scrambled beacon ($PP_{scrambled}B$) in which the linker is not MMP cleavable, as illustrated by confocal fluorescence microscopy: Figure 3A and B. HPLC-MS of the culture media following incubation with cells shows 2 peaks corresponding to the expected MMP cleaved fragments of $PP_{MMP}B$, Pyro-GPLG and LARK-BHQ3 (SI Figure S2). Examples of flow cytometry quantifying the fluorescence intensity of $PP_{MMP}B$ and $PP_{scrambled}B$ in cells incubated for different times are shown in Figure 3C. At all time points, the fluorescence intensity was 5- to 10-fold higher in cells incubated with $PP_{MMP}B$ than with the scrambled beacon ($p < 0.001$). The distributions and shape of the cells are largely homogeneous after incubation with the beacons, suggesting minimal toxicity (SI Figure S3).

The activation of $PP_{MMP}B$ *in vivo* was first examined in subcutaneous MT-1 xenografts, following i.v. administration of 2 mg/kg $PP_{MMP}B$, monitoring whole-body fluorescence following cleavage of $PP_{MMP}B$. A strong fluorescence signal localized within the tumor was seen in experimental animals (Figure 4A), demonstrating $PP_{MMP}B$ activation in the tumor. To further validate the *in vivo* MMP specificity, mice bearing tumors on both flanks were injected intratumorally with 2 mg/kg of either $PP_{MMP}B$ (left) or $PP_{scrambled}B$ (right) and followed over time. Initially, little fluorescence was observed in either tumor. However, at 6 h a 9-fold increase in tumor fluorescence was observed with $PP_{MMP}B$ (3.5 ± 0.02 average fluorescent counts/(s × area)) compared with $PP_{scrambled}B$ (0.4 ± 0.09

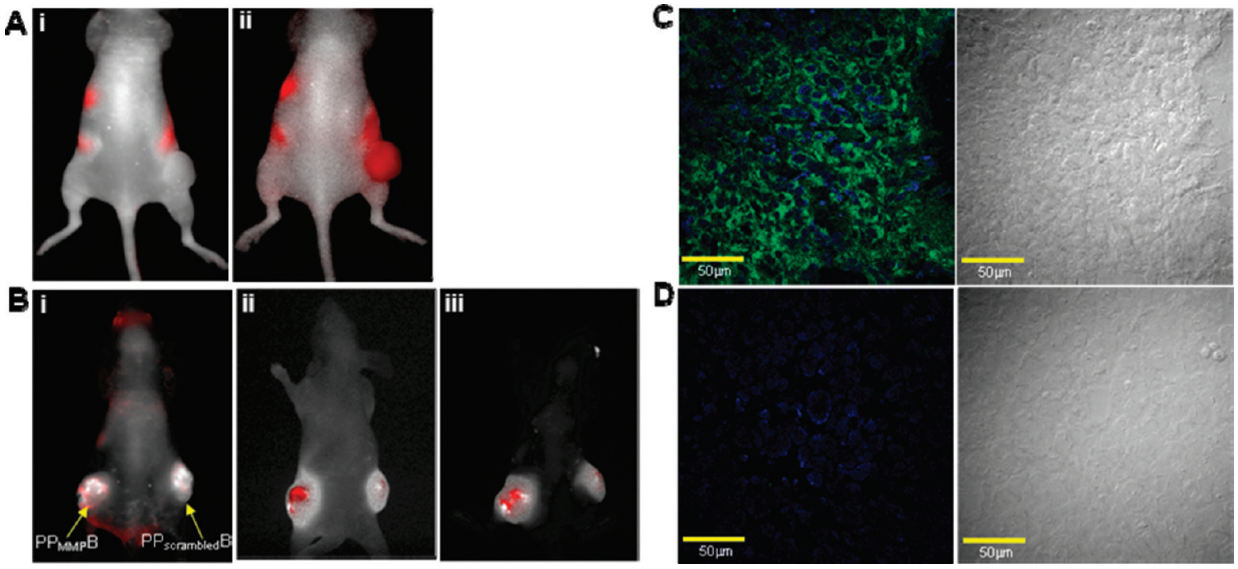

Figure 4. *In vivo* fluorescence images in the MT-1 subcutaneous xenograft tumor model: (A) before (i) and 17 h after (ii) i.v. injection of 2 mg/kg $PP_{MMP}B$ and (B) $PP_{MMP}B$ (left tumor) versus $PP_{scrambled}B$ (right tumor) images at (i) 10 min, (ii) 6 h, and (iii) 24 h post intratumor injection. Fluorescence micrographs and corresponding differential contrast images of MT-1 frozen tissue sections 24 h after administration of $PP_{MMP}B$ (C) or $PP_{scrambled}B$ (D) (n = 5, Green - activated $PP_{MMP}B$ fluorescence, DAPI - blue nucleus stain).

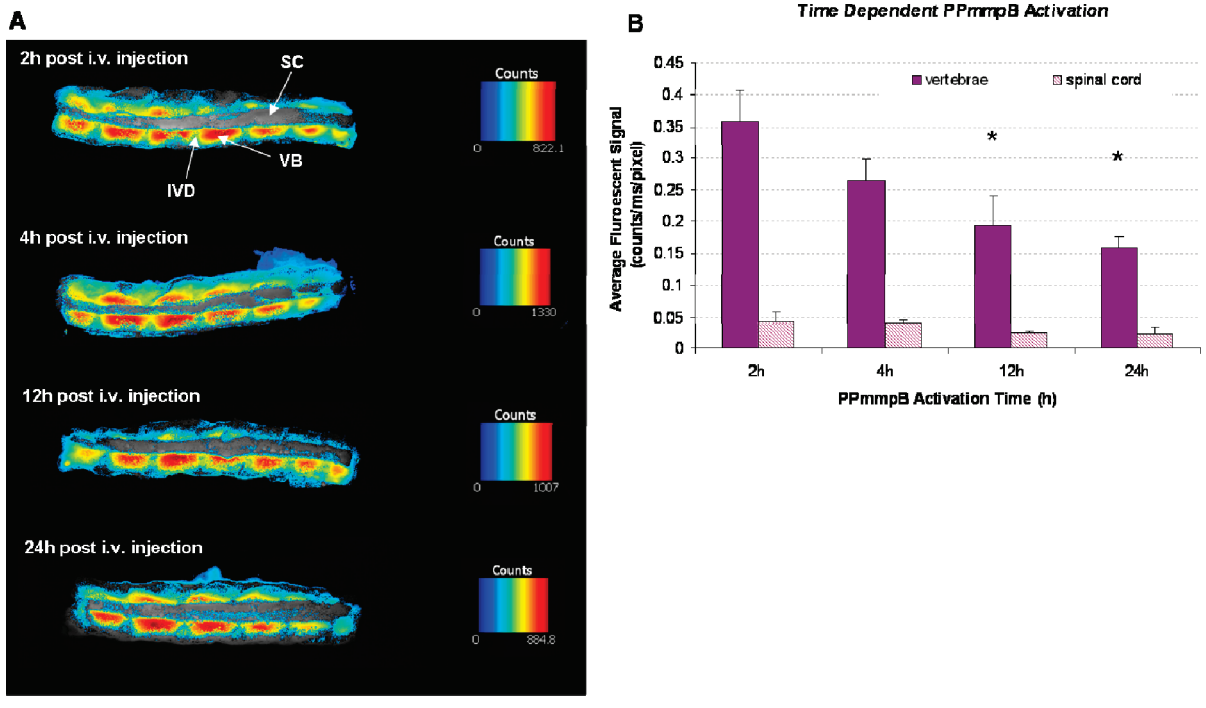

Figure 5. Time-dependent activation of $PP_{MMP}B$ by vertebral metastases imaged *ex vivo*. (A) Composite fluorescence images at 2, 4, 12, and 24 h after intravenous injection of 3 mg/kg $PP_{MMP}B$: SC – spinal cord, VB – vertebral body, IVD – intervertebral disk. (B) Average fluorescent signal comparing $PP_{MMP}B$ activation in the vertebrae and spinal cord: * indicates statistically significant difference ($p < 0.05$) in $PP_{MMP}B$ activation between vertebrae and spinal cord at all imaging time points (n = 4 for 2 and 4 h time points, n = 2 for 12 and 24 h).

average fluorescent counts/(s × area)), the latter showing minimal change in fluorescence (Figure 4B). Even after 24 h, confocal images of frozen sections of harvested tumors confirmed that fluorescence was only detectable in tumors injected with $PP_{MMP}B$ (Figure 4C).

Although these results are promising, evaluation of $PP_{MMP}B$ specific activation in veretebral metastases is necessary to validate the PDT beacon concept for this particular clinical application. Following intracardiac injection of MT-1 cells, metastatic spread to the spine was seen in all animals using bioluminescent imaging. *Ex vivo* fluorescence imaging of the sagitally cut spine over 24 h evaluated $PP_{MMP}B$ activation in vertebral metastases. As shown in Figure 5, the highest fluorescence signal was between 2 and 4 h and then significantly decreased ($p < 0.05$) at 12 and 24 h.

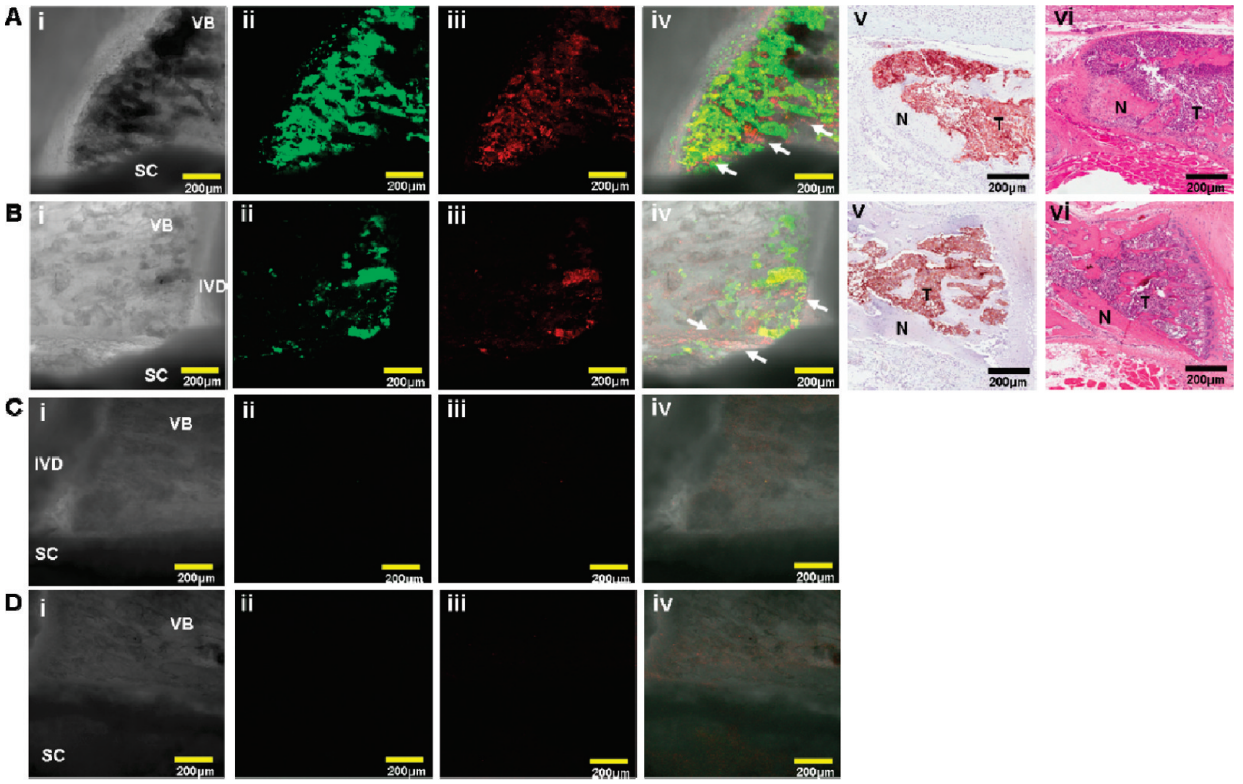

Figure 6. Micrographs of vertebrae at 2 h post i.v. injection of 3 mg/kg $PP_{MMP}B$ into (A,B) MT-1 tumor-bearing rats, (C,D) healthy rats. (i) brightfield image, (ii) GFP image showing the MT-1 cells, (iii) activated $PP_{MMP}B$, (iv) merged images of GFP and cleaved beacon (VB — vertebral body, IVD — intervertebral disk, SC — spinal cord) and corresponding (v) hEGFr and (vi) H&E stained histology sections (T —tumor, N — normal, 5× magnification). Note: in the merged images in panel iv $PP_{MMP}B$ activation extends beyond the GFP, indicating uptake/activation by surrounding tumor stroma (white arrows).

Importantly, no fluorescence signal from activated beacons was detected above background within the spinal cord at any time point (Figure 5B and SI Figure S4). Weak fluorescence was observed within the intervertebral discs (Figure 5A). The strongest fluorescence was within the vertebral body, where metastases most commonly form. At all imaging time points, the fluorescence intensity was 6- to 9-fold higher in the vertebral body versus the spinal cord ($p < 0.05$) (Figure 5B), demonstrating that $PP_{MMP}B$ activation is substantively confined to sites where vertebral metastases develop, with rapid onset of beacon activation after administration. Thus, either the beacon is not significantly taken up in or activated by the spinal cord or, at least over the time period of observation, there is no significant diffusion of cleaved $PP_{MMP}B$ activated by tumors (local or distant) into the spinal cord.

To ensure that $PP_{MMP}B$ activation was a result of the vertebral metastases expressing MMPs and not due to normal bone tissues, spines from tumor-bearing and healthy animals were imaged *ex vivo* at 2 and 4 h after i.v. administration of $PP_{MMP}B$. No fluorescence was observed in the spinal cord in either case. Under confocal microscopy, in which the unquenched beacon fluorescence was overlaid with the GFP signal of the cells, sites with positive GFP showed detectable activation (Figure 6A,B), whereas no activation was detected in the healthy animals (Figure 6C,D). Furthermore, no $PP_{MMP}B$ activation was seen within the spinal cord. The Pearson coefficients for the degree of overlap between $PP_{MMP}B$ activation and MT-1 vertebral tumors (Figure 6A,B and SI Figure S5) were 0.76 and 0.68 at 2 and 4 h post injection, respectively. This was not applicable in the healthy animal cohort, since no signal was detected in either imaging channel (tumor or cleaved beacon).

DISCUSSION

These data demonstrate that specific activation (enzymatic cleavage resulting in unquenching of the photosensitizer fluorescence) of $PP_{MMP}Bs$ is mediated by breast cancer vertebral metastases that express MMPs. Among the MMPs, other than MMP 7, $PP_{MMP}B$'s peptide linker sequence, GPLGLA, can also be specifically cleaved by MMP 10 and MMP 12, although at a lower rate than MMP 7 (data not shown). However, this additional cleavage would not be a disadvantage in this application, since both MMP 10 and 12 also play roles in bone development and bone matrix solubilization.[32−35] Since tumor cells have already hijacked the normal osteolytic cycle, MMP 10 and 12-mediated beacon activation may then aid in further disrupting the vicious tumor-bone cycle. The *in vitro* studies confirm this specific activation by the MT-1 breast cancer cells. The *in vivo* experiments in MT-1 xenografts demonstrate specific activation of $PP_{MMP}B$ by these tumors, using both systemic (i.v.) and intratumoral injection of the beacon. In the more clinically relevant metastatic model, fluorescent imaging also confirmed tumor-specific activation of $PP_{MMP}B$. There are, however, limitations with this model. The attenuation of the fluorescent signal by the overlying bone and soft tissue confounds quantitative *in vivo* imaging to determine the activation kinetics. Nevertheless, this could be determined by imaging the sectioned vertebrae *ex vivo*, albeit at only select time points, and showed that the beacon can reach and target

the intravertebral tumor tissue. In addition, it remained inactive (uncleaved) within the spinal cord, which is the critical dose-limiting tissue. It may be anticipated then that $PP_{MMP}Bs$ may serve as both a vertebral metastases-specific imaging agent and a directed PDT agent, and thus, there are a number of potential applications of $PP_{MMP}Bs$ in the treatment of patients with spinal metastases.

Surgical debulking is currently a main treatment option for spinal metastases, but recurrence is common due to incomplete resection. The strong fluorescence signal and specificity of $PP_{MMP}B$ could enable intraoperative image guidance to increase the completeness of resection and to aid in the intraoperative detection of small metastatic lesions that are otherwise not visible. Thereby, the risk of recurrence would be reduced. This is also analogous to fluorescence image-guided tumor resection in other organs.[18,36−41] Original protease activatable probes were developed to differentiate tumor versus healthy tissue, better defining surgical margins.[42−45] Thus, the initial *in vivo* and clinical application of beacons was intended for fluorescence image-guided tumor resection.[19,43,45−48] We have demonstrated tumor-specific activation for both systemic and local administration in tumor xenografts. Intratumoral injection was not technically feasible in the vertebral metastasis model due to the size limitation, but this will not be the case in patients. It is encouraging that activation occurs fairly rapidly, so that the beacon could be administered shortly before or during surgery, assuming comparable activation kinetics in humans after a local injection at the tumor site.

Furthermore, since pyropheophorbide-α is a potent PDT agent[17,24] in addition to being a fluorescence marker, PDT could be used as a means to "clean up" the surgical bed following resection, as has been used in gliomas with conventional photosensitizers.[36,49] The high degree of quenching in the intact beacon (>99%) and the tumor specificity of activation are then distinct advantages, by markedly reducing the risk of collateral damage to normal tissues that are within range of the photoactivating light. Thus, PDT treatment of the entire surgical bed post resection could result in the eradication of any residual tumor mass and microscopic vertebral metastatic deposits, while preserving normal tissues, specifically the spinal cord. Furthermore, based upon the confocal imaging of tumor cell GFP and beacon activation in vertebral metastases (Figure 6Aiv and Biv), there is evidence of beacon uptake by tumor stroma as well as by the tumor cells themselves. This is not too surprising, since it is known that MMPs are also secreted by tumor stroma.[4,5] This multicompartment targeting provides a further means to interrupt the signaling between the stroma and adjacent cancer cells by identifying cells hijacked by the tumor to promote osteolysis. Hence, eradication of the tumor microenvironment could result in further synergistic effects.

The metastases-specific activation of $PP_{MMP}B$ with its ability to remain inactive in critical normal tissues (i.e., spinal cord) combined with the potent PDT capability of Pyro in beacons makes $PP_{MMP}B$ highly attractive by providing an additional mechanism of selectivity in PDT. [17,24] PDT has been proposed as a promising therapeutic strategy for patients suffering from spinal metastases. It is an approved cancer treatment modality with several potential advantages over current cancer treatments due to its minimally invasive nature, selectivity, ability to treat patients with repeated doses without initiating resistance or exceeding total-dose limitations, fast healing that results in little or no scarring, the ability to administer in an outpatient setting, minimal associated side effects, and lack of contraindication with other modalities.[18−20] We have previously proposed and reported several preclinical studies on the concept of using PDT for destroying spinal metastases, particularly to debulk lesions as an adjuvant to vertebroplasty or kyphoplasty in order to mechanically stabilize weak or fractured vertebrae:[23,27,30,31,50,51] These surgical procedures involve injection of a plastic compound or placement of an inflatable balloon into the vertebral body, which is often limited by the space-occupying tumor mass. We have shown that not only can PDT (using the clinical photosensitizer Visudyne) ablate spinal metastatic tumors,[23] but unexpectedly it also enhances vertebral mechanical stability.[30,31] This has led to a phase I clinical trial with the clinically approved photosensitzer Visudyne (QLT Inc., Vancouver, BC, Canada), in which the objective is to debulk the intravertebral space-occupying tumor mass that often impedes these surgical approaches. However, current photosensitizers are limited by their nonspecific accumulation in normal tissues, e.g., Visudyne has nonspecific uptake in the spinal cord, limiting the therapeutic window which, in turn, reduces the aggressiveness of treatment in order to stay well within safe dose limits.[23,27] Clearly, preservation of spinal cord structure and function is critical in the management of vertebral metastases. $PP_{MMP}B$ potentially addresses this limitation and may be a key component in the use of PDT as a new, minimally invasive, safe, and effective therapy for the management of patients with spinal metastases. Although in this initial study we have not directly tested the photodynamic efficacy of the cleaved beacon against the tumor tissue, previous studies of a variety of PDT beacons in tumor xenograft models[17] have shown that this tracks with the fluorescence characteristics, as would be expected from the photophysics. Direct studies of the PDT effect are in progress, although a second limitation of the intracardiac-injection metastatic model is that the animals survive for only a few weeks[23] due to widespread disease, so that long-term treatment responses cannot be evaluated. Due to the small size of the animals, evaluation of the PDT effect due to an intratumoral injection of $PP_{MMP}B$ within the vertebrae is not possible.

In summary, we have demonstrated the specific activation of $PP_{MMP}B$ by MMP-expressing vertebral metastases in a relevant preclinical model illustrating defined kinetics and the ability to target intravertebral metastatic tumors with minimal uptake or activation in the spinal cord. This is a first step in the further development of such beacons and their potential translation into useful clinical tools for a range of applications.

■ ASSOCIATED CONTENT

Supporting Information. Additional figures as described in the text. This material is available free of charge via the Internet at http://pubs.acs.org.

■ AUTHOR INFORMATION

Corresponding Author

*Gang Zheng, 5-363 101 College St., Toronto, Canada M5G 1L7, 416-581-7666 (Primary); 416-581-7667 (Fax); gang.zheng@uhnres.utoronto.ca.

■ ACKNOWLEDGMENT

This work was supported by the Canadian Institutes of Health Research, DOD BCRP Predoc Award W81XWH-10-1-0115, and

Joey and Toby Tanenbaum/Brazilian Ball Chair in Prostate Cancer Research. Partial support was provided by the Princess Margaret Hospital Foundation and the Ontario Ministry of Health & Long Term care.

REFERENCES

(1) Mundy, G. R. (2002) Metastasis to bone: causes, consequences and therapeutic opportunities. *Nat. Rev. Cancer 2*, 584–93.

(2) Siclari, V. A., Guise, T. A., and Chirgwin, J. M. (2006) Molecular interactions between breast cancer cells and the bone microenvironment drive skeletal metastases. *Cancer Metastasis Rev. 25*, 621–33.

(3) Kingsley, L. A., Fournier, P. G., Chirgwin, J. M., and Guise, T. A. (2007) Molecular biology of bone metastasis. *Mol. Cancer Ther. 6*, 2609–17.

(4) Brinckerhoff, C. E., and Matrisian, L. M. (2002) Matrix metalloproteinases: a tail of a frog that became a prince. *Nat. Rev. Mol. Cell Biol. 3*, 207–14.

(5) Kessenbrock, K., Plaks, V., and Werb, Z. Matrix metalloproteinases: regulators of the tumor microenvironment. *Cell 141*, 52-67.

(6) Woodward, J. K., Holen, I., Coleman, R. E., and Buttle, D. J. (2007) The roles of proteolytic enzymes in the development of tumour-induced bone disease in breast and prostate cancer. *Bone 41*, 912–27.

(7) Guise, T. A. (2009) Breaking down bone: new insight into site-specific mechanisms of breast cancer osteolysis mediated by metalloproteinases. *Genes Dev. 23*, 2117–23.

(8) Yu, Q., and Stamenkovic, I. (2004) Transforming growth factor-beta facilitates breast carcinoma metastasis by promoting tumor cell survival. *Clin. Exp. Metastasis 21*, 235–42.

(9) Kasper, G., Reule, M., Tschirschmann, M., Dankert, N., Stout-Weider, K., Lauster, R., Schrock, E., Mennerich, D., Duda, G. N., and Lehmann, K. E. (2007) Stromelysin-3 over-expression enhances tumourigenesis in MCF-7 and MDA-MB-231 breast cancer cell lines: involvement of the IGF-1 signalling pathway. *BMC Cancer 7*, 12.

(10) Noe, V., Fingleton, B., Jacobs, K., Crawford, H. C., Vermeulen, S., Steelant, W., Bruyneel, E., Matrisian, L. M., and Mareel, M. (2001) Release of an invasion promoter E-cadherin fragment by matrilysin and stromelysin-1. *J Cell Sci 114*, 111–118.

(11) Lynch, C. C., Hikosaka, A., Acuff, H. B., Martin, M. D., Kawai, N., Singh, R. K., Vargo-Gogola, T. C., Begtrup, J. L., Peterson, T. E., Fingleton, B., Shirai, T., Matrisian, L. M., and Futakuchi, M. (2005) MMP-7 promotes prostate cancer-induced osteolysis via the solubilization of RANKL. *Cancer Cell 7*, 485–96.

(12) Egeblad, M., and Werb, Z. (2002) New functions for the matrix metalloproteinases in cancer progression. *Nat. Rev. Cancer 2*, 161–74.

(13) Page-McCaw, A., Ewald, A. J., and Werb, Z. (2007) Matrix metalloproteinases and the regulation of tissue remodelling. *Nat. Rev. Mol. Cell. Biol. 8*, 221–33.

(14) American Cancer Society. *Breast Cancer Facts & Figures* 2009−2010. Atlanta: American Cancer Society, I.

(15) Finn, M. A., Vrionis, F. D., and Schmidt, M. H. (2007) Spinal radiosurgery for metastatic disease of the spine. *Cancer Control 14*, 405–11.

(16) Bartels, R. H., van der Linden, Y. M., and van der Graaf, W. T. (2008) Spinal extradural metastasis: review of current treatment options. *CA Cancer J. Clin. 58*, 245–59.

(17) Zheng, G., Chen, J., Stefflova, K., Jarvi, M., Li, H., and Wilson, B. C. (2007) Photodynamic molecular beacon as an activatable photosensitizer based on protease-controlled singlet oxygen quenching and activation. *Proc. Natl. Acad. Sci. U.S.A. 104*, 8989–94.

(18) Wilson, B. C., and Patterson, M. S. (2008) The physics, biophysics and technology of photodynamic therapy. *Phys. Med. Biol. 53*, R61–109.

(19) Celli, J. P., Spring, B. Q., Rizvi, I., Evans, C. L., Samkoe, K. S., Verma, S., Pogue, B. W., and Hasan, T. (2010) Imaging and photodynamic therapy: mechanisms, monitoring, and optimization. *Chem. Rev. 110*, 2795–838.

(20) Pervaiz, S., and Olivo, M. (2006) Art and science of photodynamic therapy. *Clin. Exp. Pharmacol. Physiol. 33*, 551–6.

(21) Kohrmann, A., Kammerer, U., Kapp, M., Dietl, J., and Anacker, J. (2009) Expression of matrix metalloproteinases (MMPs) in primary human breast cancer and breast cancer cell lines: New findings and review of the literature. *BMC Cancer 9*, 188.

(22) Giambernardi, T. A., Grant, G. M., Taylor, G. P., Hay, R. J., Maher, V. M., McCormick, J. J., and Klebe, R. J. (1998) Overview of matrix metalloproteinase expression in cultured human cells. *Matrix Biol. 16*, 483–96.

(23) Akens, M. K., Hardisty, M. R., Wilson, B. C., Schwock, J., Whyne, C. M., Burch, S., and Yee, A. J. (2010) Defining the therapeutic window of vertebral photodynamic therapy in a murine pre-clinical model of breast cancer metastasis using the photosensitizer BPD-MA (Verteporfin). *Breast Cancer Res. Treat. 119*, 325–33.

(24) Lo, P. C., Chen, J., Stefflova, K., Warren, M. S., Navab, R., Bandarchi, B., Mullins, S., Tsao, M., Cheng, J. D., and Zheng, G. (2009) Photodynamic molecular beacon triggered by fibroblast activation protein on cancer-associated fibroblasts for diagnosis and treatment of epithelial cancers. *J. Med. Chem. 52*, 358–68.

(25) Engebraaten, O., and Fodstad, O. (1999) Site-specific experimental metastasis patterns of two human breast cancer cell lines in nude rats. *Int. J. Cancer 82*, 219–25.

(26) Engebraaten, O., Sivam, G., Juell, S., and Fodstad, O. (2000) Systemic immunotoxin treatment inhibits formation of human breast cancer metastasis and tumor growth in nude rats. *Int. J. Cancer 88*, 970–6.

(27) Akens, M. K., Yee, A. J., Wilson, B. C., Burch, S., Johnson, C. L., Lilge, L., and Bisland, S. K. (2007) Photodynamic therapy of vertebral metastases: evaluating tumor-to-neural tissue uptake of BPD-MA and ALA-PpIX in a murine model of metastatic human breast carcinoma. *Photochem. Photobiol. 83*, 1034–9.

(28) Klerk, C. P., Overmeer, R. M., Niers, T. M., Versteeg, H. H., Richel, D. J., Buckle, T., Van Noorden, C. J., and van Tellingen, O. (2007) Validity of bioluminescence measurements for noninvasive in vivo imaging of tumor load in small animals. *Biotechniques 43* (7−13), 30.

(29) Sato, A., Klaunberg, B., and Tolwani, R. (2004) In vivo bioluminescence imaging. *Comp. Med. 54*, 631–4.

(30) Won, E., Akens, M. K., Hardisty, M. R., Burch, S., Bisland, S. K., Yee, A. J., Wilson, B. C., and Whyne, C. M. (2010) Effects of photodynamic therapy on the structural integrity of vertebral bone. *Spine (Phila Pa 1976) 35*, 272–7.

(31) Won, E., Wise-Milestone, L., Akens, M. K., Burch, S., Yee, A. J., Wilson, B. C., and Whyne, C. M. (2010) Beyond bisphosphonates: photodynamic therapy structurally augments metastatically involved vertebrae and destroys tumor tissue. *Breast Cancer Res. Treat.*

(32) Nabha, S. M., dos Santos, E. B., Yamamoto, H. A., Belizi, A., Dong, Z., Meng, H., Saliganan, A., Sabbota, A., Bonfil, R. D., and Cher, M. L. (2008) Bone marrow stromal cells enhance prostate cancer cell invasion through type I collagen in an MMP-12 dependent manner. *Int. J. Cancer 122*, 2482–90.

(33) Hou, P., Troen, T., Ovejero, M. C., Kirkegaard, T., Andersen, T. L., Byrjalsen, I., Ferreras, M., Sato, T., Shapiro, S. D., Foged, N. T., and Delaisse, J. M. (2004) Matrix metalloproteinase-12 (MMP-12) in osteoclasts: new lesson on the involvement of MMPs in bone resorption. *Bone 34*, 37–47.

(34) Bord, S., Horner, A., Hembry, R. M., and Compston, J. E. (1998) Stromelysin-1 (MMP-3) and stromelysin-2 (MMP-10) expression in developing human bone: potential roles in skeletal development. *Bone 23*, 7–12.

(35) Andersen, T. L., del Carmen Ovejero, M., Kirkegaard, T., Lenhard, T., Foged, N. T., and Delaisse, J. M. (2004) A scrutiny of matrix metalloproteinases in osteoclasts: evidence for heterogeneity and for the presence of MMPs synthesized by other cells. *Bone 35*, 1107–19.

(36) Bogaards, A., Varma, A., Zhang, K., Zach, D., Bisland, S. K., Moriyama, E. H., Lilge, L., Muller, P. J., and Wilson, B. C. (2005) Fluorescence image-guided brain tumour resection with adjuvant metronomic photodynamic therapy: pre-clinical model and technology development. *Photochem. Photobiol. Sci. 4*, 438–42.

(37) Troyan, S. L., Kianzad, V., Gibbs-Strauss, S. L., Gioux, S., Matsui, A., Oketokoun, R., Ngo, L., Khamene, A., Azar, F., and Frangioni, J. V. (2009) The FLARE intraoperative near-infrared fluorescence imaging system: a first-in-human clinical trial in breast cancer sentinel lymph node mapping. *Ann. Surg. Oncol. 16*, 2943–52.

(38) Stenzl, A., Burger, M., Fradet, Y., Mynderse, L. A., Soloway, M. S., Witjes, J. A., Kriegmair, M., Karl, A., Shen, Y., and Grossman, H. B. (2010) Hexaminolevulinate guided fluorescence cystoscopy reduces recurrence in patients with nonmuscle invasive bladder cancer. *J. Urol. 184*, 1907–13.

(39) Upile, T., Jerjes, W., Sterenborg, H. J., El-Naggar, A. K., Sandison, A., Witjes, M. J., Biel, M. A., Bigio, I., Wong, B. J., Gillenwater, A., MacRobert, A. J., Robinson, D. J., Betz, C. S., Stepp, H., Bolotine, L., McKenzie, G., Mosse, C. A., Barr, H., Chen, Z., Berg, K., D'Cruz, A. K., Stone, N., Kendall, C., Fisher, S., Leunig, A., Olivo, M., Richards-Kortum, R., Soo, K. C., Bagnato, V., Choo-Smith, L. P., Svanberg, K., Tan, I. B., Wilson, B. C., Wolfsen, H., Yodh, A. G., and Hopper, C. (2009) Head & neck optical diagnostics: vision of the future of surgery. *Head Neck Oncol. 1*, 25.

(40) Wilson, B. C. (2007) Detection and treatment of dysplasia in Barrett's esophagus: a pivotal challenge in translating biophotonics from bench to bedside. *J. Biomed. Opt. 12*, 051401.

(41) Gibbs-Strauss, S. L., O'Hara, J. A., Hoopes, P. J., Hasan, T., and Pogue, B. W. (2009) Noninvasive measurement of aminolevulinic acid-induced protoporphyrin IX fluorescence allowing detection of murine glioma in vivo. *J. Biomed. Opt. 14*, 014007.

(42) Campo, M. A., Gabriel, D., Kucera, P., Gurny, R., and Lange, N. (2007) Polymeric photosensitizer prodrugs for photodynamic therapy. *Photochem. Photobiol. 83*, 958–65.

(43) Weissleder, R., Tung, C. H., Mahmood, U., and Bogdanov, A., Jr. (1999) In vivo imaging of tumors with protease-activated near-infrared fluorescent probes. *Nat. Biotechnol. 17*, 375–8.

(44) Bullok, K., and Piwnica-Worms, D. (2005) Synthesis and characterization of a small, membrane-permeant, caspase-activatable far-red fluorescent peptide for imaging apoptosis. *J. Med. Chem. 48*, 5404–7.

(45) McIntyre, J. O., Fingleton, B., Wells, K. S., Piston, D. W., Lynch, C. C., Gautam, S., and Matrisian, L. M. (2004) Development of a novel fluorogenic proteolytic beacon for in vivo detection and imaging of tumour-associated matrix metalloproteinase-7 activity. *Biochem. J. 377*, 617–28.

(46) Jiang, T., Olson, E. S., Nguyen, Q. T., Roy, M., Jennings, P. A., and Tsien, R. Y. (2004) Tumor imaging by means of proteolytic activation of cell-penetrating peptides. *Proc. Natl. Acad. Sci. U.S.A. 101*, 17867–72.

(47) Weissleder, R., and Ntziachristos, V. (2003) Shedding light onto live molecular targets. *Nat. Med. 9*, 123–8.

(48) Lee, S., Xie, J., and Chen, X. (2010) Activatable molecular probes for cancer imaging. *Curr. Top. Med. Chem. 10*, 1135–44.

(49) Muller, P. J., and Wilson, B. C. (2006) Photodynamic therapy of brain tumors--a work in progress. *Lasers Surg. Med. 38*, 384–9.

(50) Burch, S., Bisland, S. K., Bogaards, A., Yee, A. J., Whyne, C. M., Finkelstein, J. A., and Wilson, B. C. (2005) Photodynamic therapy for the treatment of vertebral metastases in a rat model of human breast carcinoma. *J. Orthop. Res. 23*, 995–1003.

(51) Burch, S., Bogaards, A., Siewerdsen, J., Moseley, D., Yee, A., Finkelstein, J., Weersink, R., Wilson, B. C., and Bisland, S. K. (2005) Photodynamic therapy for the treatment of metastatic lesions in bone: studies in rat and porcine models. *J. Biomed. Opt. 10*, 034011.

IVYSPRING INTERNATIONAL PUBLISHER

Theranostics

2011; 1:363-370

Research Paper

Transforming a Targeted Porphyrin Theranostic Agent into a PET Imaging Probe for Cancer

Jiyun Shi[1,2,3]*, Tracy W.B. Liu[1,2]*, Juan Chen[2], David Green[2], David Jaffray[1,2], Brian C. Wilson[1,2], Fan Wang[3] and Gang Zheng[1,2] ✉

1. Department of Medical Biophysics, University of Toronto, Toronto, Canada;
2. Ontario Cancer Institute, University Health Network, Toronto, Canada;
3. Medical Isotopes Research Center, Peking University, Beijing, China.

* J. Shi and T. Liu contributed equally to this work.

✉ Corresponding author: Gang Zheng, PhD, University of Toronto, 101 College Street, TMDT 5-363, Toronto, ON M5G1L7, Canada. Tel: 416-581-7666; Fax: 416-581-7667; E-mail: gang.zheng@uhnres.utoronto.ca

Received: 2011.07.27; Accepted: 2011.08.27; Published: 2011.09.15

Abstract

Porphyrin based photosensitizers are useful agents for photodynamic therapy (PDT) and fluorescence imaging of cancer. Porphyrins are also excellent metal chelators forming highly stable metallo-complexes making them efficient delivery vehicles for radioisotopes. Here we investigated the possibility of incorporating ^{64}Cu into a porphyrin-peptide-folate (PPF) probe developed previously as folate receptor (FR) targeted fluorescent/PDT agent, and evaluated the potential of turning the resulting ^{64}Cu-PPF into a positron emission tomography (PET) probe for cancer imaging. Noninvasive PET imaging followed by radioassay evaluated the tumor accumulation, pharmacokinetics and biodistribution of ^{64}Cu-PPF. ^{64}Cu-PPF uptake in FR-positive tumors was visible on small-animal PET images with high tumor-to-muscle ratio (8.88 ± 3.60) observed after 24 h. Competitive blocking studies confirmed the FR-mediated tracer uptake by the tumor. The ease of efficient ^{64}Cu-radiolabeling of PPF while retaining its favorable biodistribution, pharmacokinetics and selective tumor uptake, provides a robust strategy to transform tumor-targeted porphyrin-based photosensitizers into PET imaging probes.

Key words: Copper-64, Porphyrin, PET, Folate receptor, Peptides

Introduction

Porphyrins represent one of the oldest, most widely studied chemical structures, both in nature and in biomedical applications [1-2]. Due to their favorable photophysical properties, such as long wavelength absorption and emission, easy derivatization, high singlet oxygen quantum yield and low *in vivo* toxicity, porphyrins have found particular success for photodynamic therapy (PDT) and fluorescence imaging of cancer [3-6]. Several thorough reviews discussing the advantages of porphyrins as photosensitizers in photodynamic therapy may be found elsewhere [3, 5, 7]. Additionally, porphyrins are excellent metal chelators, forming highly stable metallo-complexes [8]. With the well-established stable chelation of Cu^{2+} to porphyrins, the potential use of ^{64}Cu-porphyrin for the detection of cancer in patients was recognized well over half a century ago [9]. The radioactive ^{64}Cu-porphyrin is extremely stable to

demetallation and was first used *in vivo* in 1951 to develop coincident scintillation counters permitting more accurate localization of radioisotopes [10]. Despite the emerging recognition of ^{64}Cu as a suitable radionuclide ($t_{1/2}$ = 12.7 h, β^+: 17.4%, $E_{\beta+max}$ = 656 keV; β^-: 39%, $E_{\beta-max}$ = 573 keV) in positron emitting tomography (PET) imaging [11-12], there have been few efforts and even less promising results to date for using ^{64}Cu-labeled porphyrins as PET probes [13-15]. In large part this is due to their poor tumor targeting, as well as the technical limitations of earlier PET scanners. The field went into hiatus until the 1980s when Wilson *et al*. attempted to detect brain tumors using ^{64}Cu-porphyrin with the emerging technology of PET. This effort failed to generate wide interest, due to the limited tumor localization of the particular ^{64}Cu-porphyrin and the poor spatial resolution (8 mm) of PET scanners at that time [13-14]. However, a critical result from this study was that ^{64}Cu-labeling did not alter the main characteristics (biodistribution, pharmacokinetics, clearance) of the host porphyrin molecules [13]. Although there were sporadic efforts subsequently [15-16], the overall common understanding of ^{64}Cu-porphyrins' relative inability to detect cancer remains unchallenged.

We have previously developed a folate receptor (FR)-targeted optical imaging and PDT agent, porphyrin-GDEVDGSGK-folate (PPF, Figure 1) [17]. PPF is composed of three modules: 1) pyropheophorbide-α (Pyro), a near-infrared fluorescent porphyrin, 2) folate for targeted delivery of Pyro to FR-expressing cancer cells, and 3) a short peptide as a pharmacokinetics modifying (PKM) linker. We have demonstrated, both *in vitro* and *in vivo*, that the use of three functional modules significantly improved tumor uptake efficiency, pharmacokinetics and biodistribution of the porphyrin moiety itself [17]. Here we hypothesize that incorporating ^{64}Cu into the Pyro moiety of PPF (^{64}Cu-PPF) will effectively switch PPF from a targeted fluorescent/PDT agent into a PET probe for cancer imaging. Porphyrins have several ideal characteristics as ^{64}Cu chelators: their aforementioned stable ^{64}Cu-chelating ability [10] the clinically-validated minimal toxicity of ^{64}Cu-prophyrin [9], the compatible half-lives of ^{64}Cu and the pharmacokinetics of porphyrin [13-14], and the fact that ^{64}Cu-chelation does not alter the biodistribution of the host porphyrin [13, 18]. We envision that these features of ^{64}Cu-prophyrin, coupled with the promising tumor targeting ability of PPF (Supplementary Material: Figure S1) and the high resolution and deep tissue imaging capability of modern PET technology [19-21], will enable ^{64}Cu-PPF to 1) become a novel cancer-targeted PET imaging probe, 2) facilitate the development of photosensitizers via quantitative biodistribution and pharmacokinetics assessment, 3) serve as a novel means to monitor porphyrin tumor uptake in patients receiving PDT, either by pre-treatment PET scanning or by administering a cocktail of labeled and unlabelled porphyrin and, most importantly 4) open the door to transform a variety of porphyrin photosensitizers into PET probes [22-23].

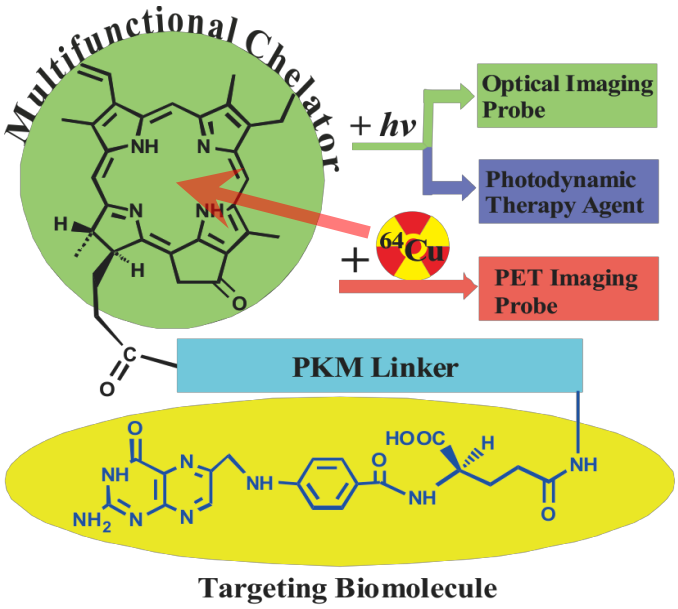

Figure 1. The structure design of the PPF (Pyro-PKM Linker-Folate, molecular weight of 1800 g/mol). Here the PKM linker (pharmacokinetics modifying linker) is the peptide sequence, GDEVDGSGK.

Experimental Section

^{64}Cu-Radiolabeling: In a 1.5 mL eppendorf tube, 2 μL DMSO was added to dissolve 50 μg (~30 nmol) of PPF (Pyro-Peptide-Folate). 0.1 mL of 0.1 M NH_4OAc buffer (pH = 5.5) was added and vortexed, producing a dark green solution. 0.10 mL of ^{64}Cu(Acetate)$_2$ solution (0.5 - 5.0 mCi) was then added and the reaction mixture was heated in a water bath at 60 °C for 20 min. After cooling to room temperature, a sample of resulting solution was analyzed by radio-UPLC.

The radio-UPLC method: The radio-UPLC method used the Acquity™ Waters UPLC system (Waters Corp., Milford, MA) equipped with PDA detector and Bioscan radioactive detector and Acquity BEH C18 column (2.1 × 100 mm, 1.7 μm; Waters). The flow rate was 0.8 mL/min. The mobile phase was isocratic with 80% solvent A (0.1 M TEAA, pH 7) and

20% solvent B (acetonitrile) at 0 min, followed by a gradient mobile phase shifting from 20% solvent B at 0 min to 100% solvent B at 12 min and back to 20% solvent B at 13-15 min.

Purification: Purification with Sep-Pak C18 cartridge was done according to the following procedures: 1) Attach a syringe to the Sep-Pak C18 cartridge. 2) Flush the column with 5 mL of ethanol and flush the column with 10 mL of saline to equilibrate the column. 3) Load the sample onto the column and wash the sample with 10 mL of saline. 4) Elute with 400 µl of 80% ethanol, collect the fractions of purified sample. 5) Dry samples using a speed-vacuum and resuspend in saline. A certain amount of radioactive is washed down in step 3 if unlabeled free ^{64}Cu is observed in the system. With the natural dark green color of Pyro, the elution of Pyro-conjugate can be easily and directly monitored visually in step 4, and the fractions with the deepest color contain the highest concentration of labeled and unlabeled Pyro-conjugate.

Dose Preparation: ^{64}Cu-PPF was prepared and administered without any further purification. The dose solution was prepared by dissolving the radiotracer in saline to a concentration of 2.5 - 5.0 mCi/mL for MicroPET imaging, and diluted to a concentration of 0.1 - 0.5 mCi/mL. The resulting solution was filtered with a 0.20 µMillex-LG filter before being administered to the animals. Each tumor-bearing mouse was injected via the tail vein with 0.1 - 0.2 mL of the filtered dose solution.

Solution Stability: For *in vitro* solution stability studies, ^{64}Cu-PPF was prepared and used without any further purification. The ^{64}Cu-PPF was dissolved in a saline or serum solution (10% FBS in saline) with a final amount of 1 mCi/mL and left at room temperature for stability measurements. Samples of the resulting solution were analyzed by radio-UPLC at 0, 6, and 24 h post-incubation. The samples from the serum solution were centrifuged before UPLC injection.

***In vivo* xenograft model:** All animal studies were carried out under institutional approval (University Health Network, Toronto, Canada). Adult athymic female nude mice were inoculated subcutaneously with 1x10^6 of KB (FR-positive human epidermal cancer) or MT-1 (FR-positive human breast carcinoma) cells in 200 µL of media in the left flank under general anesthesia with 2% isoflurane in oxygen. Animals were maintained in pathogen-free conditions in autoclaved microisolator cages. After 2 weeks, the tumors were 5-10 mm in diameter.

MicroPET/CT Imaging. MicroPET imaging was performed using a MicroPET R4 rodent model scanner (Concorde Microsystems, Knoxville, TN). The tumor-bearing mice (n = 3) were anesthetized with 2% isoflurane in oxygen, and injected with ~500 µCi of ^{64}Cu-PPF via the tail vein, and placed near the center of the FOV where the highest resolution and sensitivity are obtained. A 10-min static PET image was obtained at 4 h post injection and 30-45 min static PET images were acquired at 24 h post injection. Throughout the imaging, mice were kept anesthetized and directly transferred to the scanner, together with the supporting bed, without any movement. CT scanning was carried out immediately after each PET imaging session. For the blocking experiment, a mouse bearing a KB xenograft was injected with 500 µCi of ^{64}Cu-PPF along with 500-fold excess free folic acid. The static PET images were then acquired with same parameters at 4 and 24 h post injection.

Biodistribution Studies: Biodistribution studies were performed using the athymic nude mice bearing KB xenografts. Twenty tumor-bearing mice (25 - 30 g) were randomly divided into 5 groups. The ^{64}Cu radiotracer (~12.5 µCi in 0.1 mL saline) was administered into each animal via the tail vein. Four animals were euthanized by with 2% isoflurane, exsanguinated, and opening of the thoracic cavity at 4 or 24 h post injection. Blood samples were withdrawn from the heart through a syringe. Organs were excised, washed with saline, dried with absorbent tissue, weighed and counted on a γ-counter (Perkin-Elmer Wizard-1480). Organs of interest included the tumor, heart, spleen, lungs, liver, kidneys, adrenal, stomach, intestine, muscle, bone and brain. Organ uptake was calculated as a percentage of the injected dose per gram of tissue (%ID/g). For the blocking experiment, each animal was administered with ~12.5 µCi of ^{64}Cu radiotracer along with more than 500-fold excess folic acid, and animals were sacrificed at 4 or 24 h post injection for biodistribution studies. The organ uptake (%ID/g) was compared to that obtained in the absence of excess folic acid at the same time point. The biodistribution data and target-to-background (T/B) ratios are reported as the mean and standard deviation based on results from three animals at each time point. Comparison between two different radiotracers was made using the two-way ANOVA test (GraphPad Prim 5.0, San Diego, CA). The level of significance was set at p <0.05.

Metabolism: Normal athymic nude mice (n = 2) were used to evaluate the metabolic stability of ^{64}Cu-labeled PPF. Each mouse was injected with the ^{64}Cu radiotracer at a dose of ~200 μCi in 0.1 mL of saline via the tail vein. Urine samples were collected at 1.0 h post injection by manual void and mixed with saline solution. The mixture was centrifuged at 8,000 rpm for 3 min. The supernatant was collected and

filtered through a 0.20 µm Millex-LG filter unit. The filtrate was analyzed by radio-UPLC.

Results

An important condition for receptor-targeted delivery of radiolabeled agents is the development of labeling chemistry that allows for the stable and facile preparation of radiolabeled biologically-active molecules. The half-life of ^{64}Cu ($t_{1/2}$ = 12.7 h) provides adequate time for radiolabeling chemistry and imaging over 24-48 h to accommodate PPF accumulation at targeted sites [17]. The PKM linker enhances the water solubility of PPF (Figure 1), thereby improving its cancer-specificity, since water-soluble porphyrins give assistance to increased affinity for tumor tissues [17-18]. PPF was easily dissolved in an aqueous solution with a small amount of DMSO (≤ 1%) and was radiolabeled efficiently in 0.1 M ammonium acetate buffer at 60°C for 10-20 min (Figure 2a). The success of the ^{64}Cu labeling was determined by radio-UPLC (Ultra Performance Liquid Chromatography) using a C_{18} column. Using simultaneous multichannel monitoring of the pyro-specific UV absorbance at 410 nm and a radioactive signal, the incorporation of ^{64}Cu into PPF was observed. As expected, no free ^{64}Cu was detected during the radiolabeling procedure, based on the radio-UPLC radioactive channel chromatography (Figure 2b). The radiolabeling yield was > 99.9% and the radiochemical purity of ^{64}Cu-PPF was > 98% and the specific activity was 2.66 × 10^6 GBq/mol. Milder temperatures (room temperature and 37 °C) were also evaluated but resulted in a lower radiolabeling efficiency (50-80%), even after 20-30 min incubation. In this case, C_{18}-cartridge purification removed all free ^{64}Cu (see details of method in Supporting Information) and PPF was efficiently radiolabeled with ^{64}Cu, successfully transforming the optical theranostic into a nuclear medicine tracer.

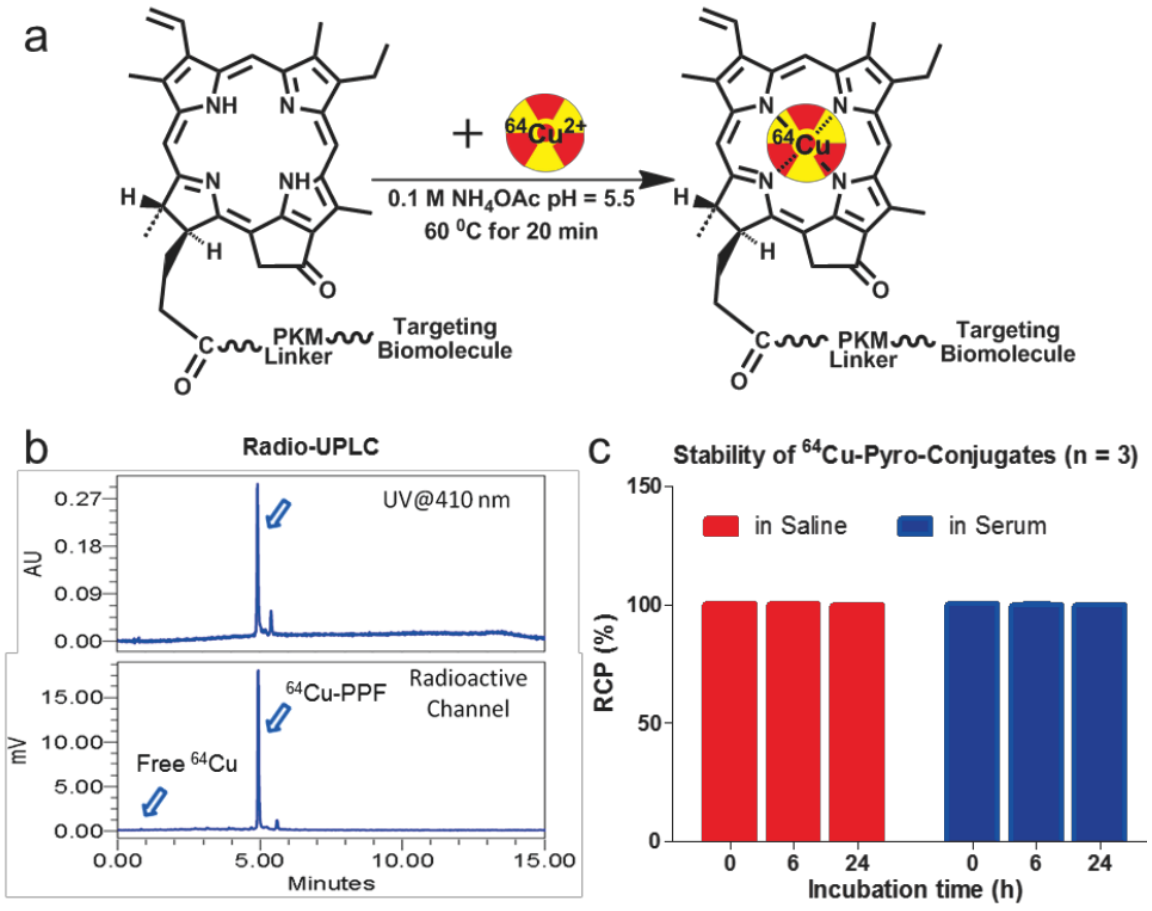

Figure 2. The radiolabeling procedure, quality control and stability of ^{64}Cu-PPF. a) The scheme of the ^{64}Cu-radiolabeling of Pyro-Conjugates, b) quality control of ^{64}Cu-labeled PPF by radio-UPLC, c) *in vitro* stability of ^{64}Cu-Pyro-Conjugates in saline or serum (10% FBS) solution (RCP = The radiochemical purity of ^{64}Cu-Pyro-Conjugates) (n = 3).

The stability of the radio-metalloporphyrin is critical to the design of a radiopharmaceutical. The ^{64}Cu-PPF stability was separately measured in both a saline and serum solution (10% FBS) for 24 h (Figure 3). These data demonstrates that the incorporation of ^{64}Cu into PPF resulted in a very stable metalloporphyrin complex. To evaluate the metabolic stability of the ^{64}Cu-PPF in vivo, athymic nude mice weighing 25-30 g were administered 200 µCi (100 µL) ^{64}Cu-PPF intravenously (tail vein). All animal studies were carried out under institutional approval (Ontario Cancer Institute, Toronto, Canada, AUP 2273.0). Urine samples were collected at 1 h post injection. Samples was centrifuged, filtered, and evaluated by radio-UPLC. The UPLC chromatogram showed one intact ^{64}Cu-PPF peak (Figure 4) indicating good metabolic stability. Only a few chelators have been reported to have both high stability and efficient radiolabeling protocols under mild conditions [24-26].

We next evaluated the potential of ^{64}Cu-PPF for PET imaging of FR expression in tumors in vivo. The FR-positive KB xenograft mouse model previously used for PPF-based optical imaging and PDT was used [17]. Animals weighing 25-30 g received a 500 µCi (~18 MBq) intravenous injection of ^{64}Cu-PPF. Cu toxicity is not a concern as the dose used for PET studies (500 µCi, ~18 MBq) is far lower than those used for radiotherapy studies in which a 10 mCi (~370 MBq) of ^{64}Cu has been administered in murine models with no overt toxicity reported [27-29]. MicroPET imaging and MicroCT scans were performed accordingly at 4 and 24 h post-injection. The favorable tumor-to-background ratio of ^{64}Cu-PPF is evident in Figure 5a. ^{64}Cu-PPF easily delineates the tumor from all other tissues by PET. Inhibition imaging studies were conducted by co-injection of the radiotracer with 500-fold excess folic acid. Figure 3b demonstrates that the uptake of ^{64}Cu-PPF at the tumor site was significantly blocked by excess folic acid, indicating that ^{64}Cu-PPF targeting is FR-mediated. Biodistribution studies of ^{64}Cu-PPF in the KB xenograft models at 4 and 24 h post-injection were also performed. All vital organs (including heart, liver, spleen, kidney, lung, stomach, large-intestine, small intestine, adrenal, brain, muscle and bone) and tumors were removed, washed with normal saline and weighed for radioassay. The highest uptake was in the kidneys, corresponding to the PET imaging results. Tumor uptake was 3.02 ± 0.55 % injected dose (ID)/g at 4 h and 1.64 ± 0.33 %ID/g at 24 h post injection (Figure 5c).

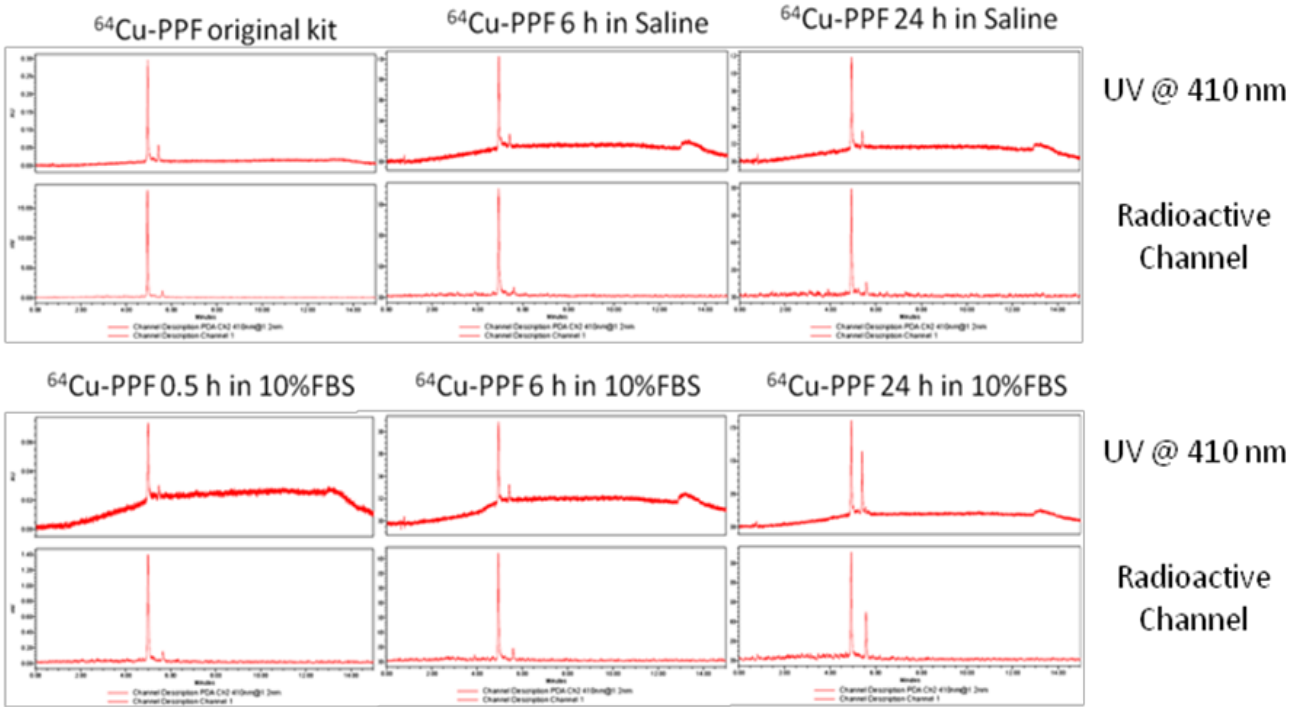

Figure 3. The *in vitro* stability of ^{64}Cu-pyropheophorbide-a conjugates in saline (a) and serum (10% FBS) (b) was measured by radio-UPLC with UV 410 nm channel and radioactivity channel. We demonstrate the stability of ^{64}Cu chelation within the porphyrin, pyropheophorbide-a. Folic acid conjugation does not affect the stability of ^{64}Cu chelation as both ^{64}Cu-PPF (major peak, with folate) and ^{64}Cu-PP (minor peak, no folate) show that ^{64}Cu complexes stably to the porphyrin as no free ^{64}Cu is observed over time.

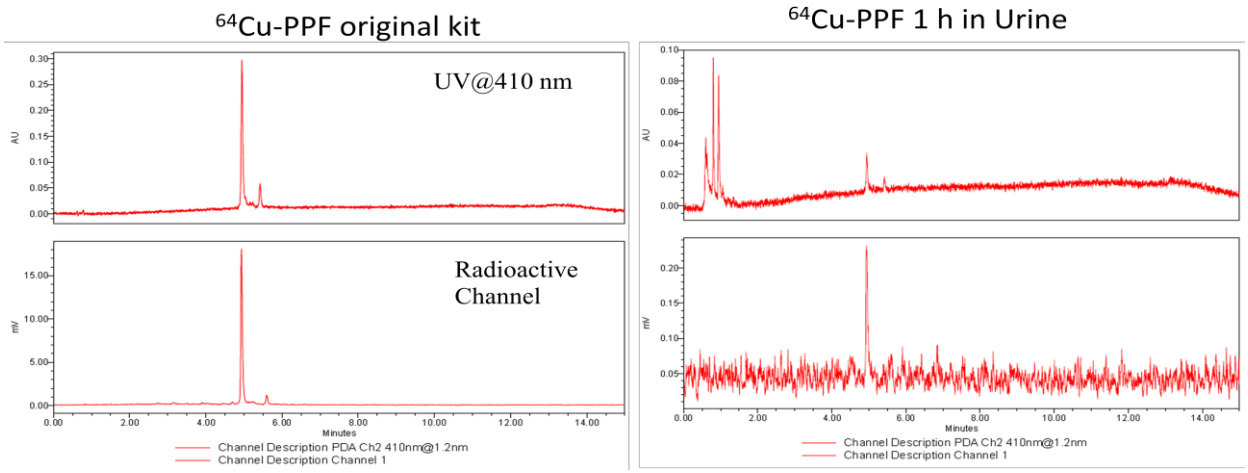

Figure 4. The metabolic stability of ^{64}Cu-PPF in urine was measured by radio-UPLC with UV 410 nm channel and radioactivity channel at 1 h post injection.

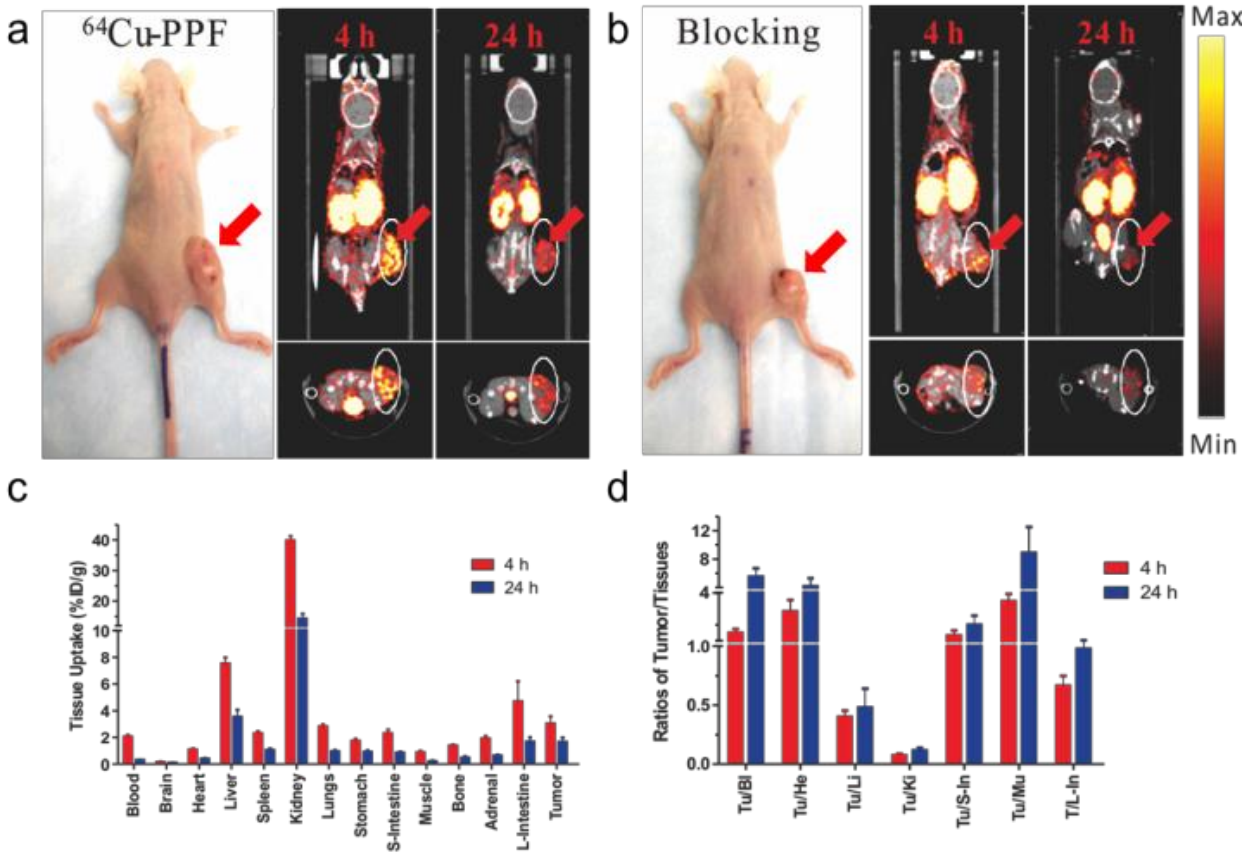

Figure 5. MicroPET/CT imaging and biodistribution. a) Representative MicroPET/CT images (coronal images (top) and single transverse slices passing through the tumors (bottom)) of KB tumor-bearing mice (n = 3) at 4, 24 h after intravenous injection of ^{64}Cu-PPF. b) Images, including coronal images (top) and single transverse slices passing through the tumors (bottom), obtained with pre-injection (0.5 h earlier) of 500-fold excess folic acid for blockade (n = 1). c) Tissue uptake of ^{64}Cu-PPF in selected organs at 4 h (red bars) and 24 h (blue bars) after intravenous injection. d) Ratios of tumor-to-selected organs in mice administered with ^{64}Cu-PPF at 4 h (red bars) and 24 h (blue bars) post injection. Data are presented as means ± 1 SD (n = 3).

However, the tumor-to-muscle ratio of ^{64}Cu-PPF was 3.47 ± 0.47 at 4 h and 8.88 ± 3.60 at 24 h post injection (Figure 5d), demonstrating the fast clearance of ^{64}Cu-PPF in non-target tissues while ^{64}Cu-PPF is retained within the tumor. Previous studies evaluating the biodistribution of ^{64}Cu-labelled hematoporphyrin derivatives demonstrated no higher than a 1.07 ± 0.25 %ID/g [14]. Blocking biodistribution studies further demonstrated the FR-specific uptake (Supplementary Material: Figure S2). Additional experiments with another FR-positive tumors confirmed these current findings (MicroPET imaging results of MT-1, a human breast cancer model, are shown in Supplementary Material: Figure S3).

Conclusions

Through the present study, we hope to revitalize this field of radio-metalloporphyrin, based on the demonstration of ^{64}Cu-PPF as a targeted PET imaging probe for FR-positive tumors. We have shown the ease and efficient radiolabeling of PPF with ^{64}Cu, while retaining its favorable biodistribution, pharmacokinetics and selective tumor uptake, characteristics that were first demonstrated optically. Clearly, the 12.7 h half-life of ^{64}Cu is compatible with the pharmacokinetics of PPF, providing adequate time for both the radiolabeling chemistry and accumulation of ^{64}Cu-PPF at tumor sites. Lastly, we report the first stable chelation of ^{64}Cu with a chlorophyll moiety, pyro. Not only is ^{64}Cu-PPF a promising diagnostic tool for FR-positive tumors, the use of ^{64}Cu-PPF may be employed for prediction and quantitative measurements of photosensitizer accumulation in tumors to aid in treatment planning and monitoring of PDT treatments. Radiolabeling PPF also provides a more accurate and quantitative measurement of the probe's *in vivo* biodistribution, due to the difficulty of absolute quantification of fluorescence *in vivo*. The ease and stable chelation of ^{64}Cu warrants further investigation of other radioisotopes more suitable for clinical PET imaging studies that may also form highly stable metalloporphyrin complexes such as ^{60}Cu and ^{62}Cu [30]. With the multifunctional properties of porphyrins and the efficient and stable incorporation of ^{64}Cu, this approach of first developing a porphyrin-based optical theranostic probe with excellent *in vivo* tumor targeting characteristics and then switching it a targeted nuclear imaging probe through chelation of a radioisotope can be translated to any targeted porphyrin-based agent.

Acknowledgements

Financial support for this work was provided by the Ontario Institute for Cancer Research, the Canadian Institute of Health Research, the DOD BCRP Predoc Award W81XWH-10-1-0115, the Natural Sciences and Engineering Research Council of Canada, the Canadian Foundation of Innovation, China "973" project (2011CB707703), NSFC project (30930030), and the Joey and Toby Tanenbaum/Brazilian Ball Chair in Prostate Cancer Research. We thank Dr. Tab Siqiddi for his help with the radio-UPLC technique.

Supplementary Material

In vivo optical imaging study using the unlabeled PPF, *in vivo* folic acid blocking study of ^{64}Cu-PPF, and MicroPET/CT imaging and biodistribution study of ^{64}Cu-PPF in a different tumor model (MT-1).
http://www.thno.org/v01p0363s1.pdf

Conflict of Interest

The authors have declared that no conflict of interest exists.

References

1. Kadish K, et al. The Porphyrin Handbook. Boston, USA: Academic Press; 2011.
2. Lovell JF, Jin CS, Huynh E, Jin H, Kim C, Rubinstein JL, et al. Porphysome nanovesicles generated by porphyrin bilayers for use as multimodal biophotonic contrast agents. Nat Mater. 2011; 10: 324-32.
3. Dougherty TJ, Gomer CJ, Henderson BW, Jori G, Kessel D, Korbelik M, et al. Photodynamic therapy. J Natl Cancer Inst. 1998; 90: 889-905.
4. Liu TW, Chen J, Zheng G. Peptide-based molecular beacons for cancer imaging and therapy. Amino acids. 2010; epub.
5. Ethirajan M, Chen Y, Joshi P, Pandey RK. The role of porphyrin chemistry in tumor imaging and photodynamic therapy. Chem Soc Rev. 2011; 40: 340-62.
6. Stefflova K, Chen J, Zheng G. Killer beacons for combined cancer imaging and therapy. Curr Med Chem. 2007; 14: 2110-25.
7. Lovell JF, Liu TW, Chen J, Zheng G. Activatable photosensitizers for imaging and therapy. Chem Rev. 2010; 110: 2839-57.
8. Ali H e al. Metal Complexes as Photo- and Radiosensitizers. Chem Rev. 1999; 99: 2379-450.
9. Bases R, Brodie SS, Rubenfeld S. Attempts at tumor localization using Cu 64-labeled copper porphyrins. Cancer. 1958; 11: 259-63.
10. Wrenn FRJr., Good ML, Handler P. The use of positron-emitting radioisotopes for the localization of brain tumors. Science. 1951; 113: 525-7.
11. Jacobson O, Weiss ID, Szajek LP, Niu G, Ma Y, Kiesewetter DO, et al. PET imaging of CXCR4 using copper-64 labeled peptide antagonist. Theranostics. 2011; 1: 251-62.
12. Zhang Y, Yang Y, Cai W. Multimodality Imaging of Integrin alpha(v)beta(3) Expression. Theranostics. 2011; 1: 135-48.
13. Firnau G, Maass D, Wilson BC, Jeeves WP. 64Cu labelling of hematoporphyrin derivative for non-invasive in-vivo measurements of tumour uptake. Prog Clin Biol Res. 1984; 170: 629-36.
14. Wilson BC, Firnau G, Jeeves WP, Brown KL, Burns-McCormick DM. Chromatographic analysis and tissue distribution of

radiocopper-labelled haematoporphyrin derivatives. Laser Med Sci. 1988; 3: 71-80.
15. Soucy-Faulkner A, et al. Copper-64 labeled sulfophthalocyanines for positron emission tomography (PET) imaging in tumor-bearing rats. Journal of Porphyrins and Phthalocyanines. 2008; 12: 49-53.
16. Roberts JC, Newmyer SL, Mercer-Smith JA, Schreyer SA, Lavallee DK. Labeling antibodies with copper radionuclides using N-4-nitrobenzyl-5-(4-carboxyphenyl)-10,15,20-tris (4-sulfophenyl) porphine. Int J Rad Appl Instrum A. 1989; 40: 775-81.
17. Stefflova K, Li H, Chen J, Zheng G. Peptide-based pharmacomodulation of a cancer-targeted optical imaging and photodynamic therapy agent. Bioconjug Chem. 2007; 18: 379-88.
18. Hambright P, Fawwaz R, Valk P, McRae J, Bearden AJ. The distribution of various water soluble radioactive metalloporphyrins in tumor bearing mice. Bioinorg Chem. 1975; 5: 87-92.
19. Gambhir SS. Molecular imaging of cancer with positron emission tomography. Nat Rev Cancer. 2002; 2: 683-93.
20. Chen X. Integrin Targeted Imaging and Therapy. Theranostics. 2011; 2011: 28-9.
21. Beer AJ, Kessler H, Wester HJ, Schwaiger M. PET Imaging of Integrin alphaVbeta3 Expression. Theranostics. 2011; 1: 48-57.
22. Zheng G, Chen J, Stefflova K, Jarvi M, Li H, Wilson BC. Photodynamic molecular beacon as an activatable photosensitizer based on protease-controlled singlet oxygen quenching and activation. Proc Natl Acad Sci U S A. 2007; 104: 8989-94.
23. Jeong H, Huh M, Lee SJ, Koo H, Kwon IC, Jeong SY, et al. Photosensitizer-conjugated human serum albumin nanoparticles for effective photodynamic therapy. Theranostics. 2011; 1: 230-9.
24. Ferreira CL, Yapp DT, Crisp S, Sutherland BW, Ng SS, Gleave M, et al. Comparison of bifunctional chelates for (64)Cu antibody imaging. Eur J Nucl Med Mol Imaging. 2010; 37: 2117-26.
25. Ferreira CL, Yapp DT, Lamsa E, Gleave M, Bensimon C, Jurek P, et al. Evaluation of novel bifunctional chelates for the development of Cu-64-based radiopharmaceuticals. Nucl Med Biol. 2008; 35: 875-82.
26. Wadas TJ, Wong EH, Weisman GR, Anderson CJ. Copper chelation chemistry and its role in copper radiopharmaceuticals. Curr Pharm Des. 2007; 13: 3-16.
27. Lewis J, Laforest R, Buettner T, Song S, Fujibayashi Y, Connett J, et al. Copper-64-diacetyl-bis(N4-methylthiosemicarbazone): An agent for radiotherapy. Proc Natl Acad Sci U S A. 2001; 98: 1206-11.
28. Lewis JS, Lewis MR, Cutler PD, Srinivasan A, Schmidt MA, Schwarz SW, et al. Radiotherapy and dosimetry of 64Cu-TETA-Tyr3-octreotate in a somatostatin receptor-positive, tumor-bearing rat model. Clin Cancer Res. 1999; 5: 3608-16.
29. Anderson CJ, Jones LA, Bass LA, Sherman EL, McCarthy DW, Cutler PD, et al. Radiotherapy, toxicity and dosimetry of copper-64-TETA-octreotide in tumor-bearing rats. J Nucl Med. 1998; 39: 1944-51.
30. Williams HA, Robinson S, Julyan P, Zweit J, Hastings D. A comparison of PET imaging characteristics of various copper radioisotopes. Eur J Nucl Med Mol Imaging. 2005; 32: 1473-80.